CHEMISTRY
AN ASIAN JOURNAL

www.chemasianj.org

A Journal of

ACES
Asian Chemical Editorial Society

REPRINT

WILEY-VCH

ACES Asian Chemical Editorial Society

DOI: 10.1002/asia.201801255

CHEMISTRY AN ASIAN JOURNAL Full Paper

Polyoxometalates | *Very Important Paper* |

VIP

Ligand-Controlled Assembly of Heteropolyoxomolybdates from Plenary Keggin Germanomolybdates and Cu–Ln Heterometallic Units

Pei-Jun Gong, Jing-Jing Pang, Hui-Fen Hu, Hui-Jie Li, Li-Juan Chen,* and Jun-Wei Zhao*[a]

Abstract: By virtue of combining an in-situ assembly process with a stepwise synthesis in conventional aqueous solution, two series of unique organic–inorganic hybrid heteropolyoxomolybdates were constructed from plenary Keggin germanomolybdates and Cu–Ln heterometallic units and fully characterized: $[H_2INA]_2H_8[LnCu(INA)_4(H_2O)_6]_2[\alpha\text{-}GeMo_{12}O_{40}]_3\cdot 52H_2O$ (Ln = La^{3+} (**1**), Ce^{3+} (**2**), Pr^{3+} (**3**), Nd^{3+} (**4**), Sm^{3+} (**5**), Eu^{3+} (**6**); HINA = isonicotinic acid) and $(NH_4)[Cu(PA)_2][Cu(PA)_2Ln(H_2O)_8][\alpha\text{-}GeMo_{12}O_{40}]\cdot 10H_2O$ (Ln = Nd^{3+} (**7**), Sm^{3+} (**8**), Eu^{3+} (**9**); HPA = picolinic acid). The most remarkable structural characteristic of compounds **1**–**6** was that their molecular units were defined by three discrete plenary Keggin $[\alpha\text{-}GeMo_{12}O_{40}]^{4-}$ polyoxoanions and two organic–inorganic hybrid heterometallic $[LnCu(INA)_4(H_2O)_6]^{+}$ moieties, whereas compounds **7**–**9** exhibited a nice-looking 1D chain-like structure that was built from plenary $[\alpha\text{-}GeMo_{12}O_{40}]^{4-}$ polyoxoanions, pendent $[Cu(PA)_2]$ complexes, and bridging $\{[Cu(PA)_2][Ln(H_2O)_8]\}^{3+}$ heterometallic groups. Notably, two different pyridine carboxylic acid ligands led to the discrepancy between the two structure types. To the best of our knowledge, compounds **1**–**9** constitute the first examples of plenary Keggin heterometallic germanomolybdates that include Cu–Ln–organic subunits. Further studies revealed that compounds **3** and **8** exhibited fast adsorption capacity for cationic dyes methylene blue (MB) and rhodamine B (RhB) in water. Moreover, compounds **3** and **8** could quickly and selectively adsorb MB from a mixture of MB/methyl orange (MO) or MB/azophloxine (Apo).

1. Introduction

In recent years, research into multifunctional crystalline materials has "mushroomed" on account of their unparalleled structural topologies and versatility, with applications in magnetism, catalysis, optics, and medicine, among others.[1] As such, polyoxometalates (POMs), as clusters of early-transition-metal oxides with rich structural diversity and high negative charges, have become one of the most rapidly developing families of compound in modern inorganic and materials chemistry,[2] and have drawn considerable interest on account of their structural aesthetic and unrivalled diversity, coupled with their tunable chemical and physical properties, in biology, catalysis, and materials science.[3] On the other hand, 3d–4f complexes are promising candidates for the construction of new functional materials and have attracted much attention, owing to their intriguing optoelectronic, magnetic, and catalytic properties.[4] Therefore, the search for new 3d–4f heterometallic (DFH) polyoxometalates (DFHPOMs) has been a significant research topic, with the profound development of multifunctional materials and relevant applications in molecular adsorption, bimetallic catalysis, and magnetism.[5] However, it remains difficult to find appropriate and rational experimental conditions for the synthesis of DFHPOMs, because 4f-metal ions exhibit more-oxophilic reactivity with POMs, often leading to amorphous precipitates rather than crystalline phases, whilst interactions between 3d-metal cations and polyoxoanions are fairly weak.[6] As a result, under the same reaction conditions, an inevitable competition reaction must occur between the strongly oxyphilic 4f-metal ions, the relatively weak reactive 3d-metal ions, and highly negative polyoxoanions.[5b,6b,c,7] Thus, the development of suitable reaction strategies for the creation of DFHPOMs is a great challenge.

The gate for DFHPOMs chemistry was first opened by the ground-breaking synthesis of $(NH_4)_{21}[Ln(H_2O)_5\{Ni(H_2O)\}_2As_4W_{40}O_{140}]\cdot nH_2O$ (Ln = Ce^{3+}, Pr^{3+}, Nd^{3+}, Sm^{3+}, Eu^{3+}, Gd^{3+}) by Xue et al. in 2004.[8] Several achievements followed[9] and, in 2007, the first sandwich-type Dy^{III}–V^{IV} heterometallic arsenotungstate complex, $Na_3K_5[((VO)_2Dy(H_2O)_4K_2(H_2O)_2Na(H_2O)_2)(\alpha\text{-}B\text{-}AsW_9O_{33})_2]\cdot 23H_2O$, was reported by Müller's group.[9a] Then, in 2008, Fang and Kögerler discovered two new Dawson-type phosphotungstate-based Ce^{IV}–Mn^{IV} heterometallic clusters, $[\{\alpha\text{-}P_2W_{15}O_{56}\}_6\{Ce_3Mn_2(\mu_3\text{-}O)_4(\mu_2\text{-}OH)_2\}_3(\mu_2\text{-}OH)_2(H_2O)_2(PO_4)]^{47-}$[9b] and [{α-

[a] P.-J. Gong, J.-J. Pang, H.-F. Hu, H.-J. Li, Dr. L.-J. Chen, Prof. J.-W. Zhao
Henan Key Laboratory of Polyoxometalate Chemistry
College of Chemistry and Chemical Engineering
Henan University
Kaifeng 475004 (P. R. China)
E-mail: ljchen@henu.edu.cn
zhaojunwei@henu.edu.cn

Supporting information and the ORCID identification number(s) for the author(s) of this article can be found under: https://doi.org/10.1002/asia.201801255.

$P_2W_{16}O_{57}(OH)_2\}\{CeMn_6O_9(O_2CCH_3)_8\}]^{8-}$.[9c] Shortly thereafter, a series of 3d–4f heterometallic polyoxotungstates that were composed of classical 1:2-type $[Ln(\alpha\text{-}XW_{11}O_{39})_2]^{n-}$ units (X = P^V, Si^{IV}, Ge^{IV}, As^V; n = 11, 13) and copper–organoamine linkers were obtained.[6d,9d–m] Recently, we have also made great efforts in this field and several classes of intriguing DFHPOMs have been isolated by our group,[9h–l,n–r] including the first purely inorganic Fe–Ln heterometallic tungstoantimonates, $[Pr(H_2O)_8][Pr(H_2O)_6][Fe_4(H_2O)_{10}(B\text{-}\beta\text{-}SbW_9O_{33})_2]\cdot 16H_2O$ and $[Ln(H_2O)_7]_2[Fe_4(H_2O)_{10}(B\text{-}\beta\text{-}SbW_9O_{33}]_2\cdot 22H_2O$ (Ln = Tb^{3+}, Dy^{3+}, Lu^{3+}),[9p] and the first organic–inorganic Fe–Ln heterometallic tungstoantimonate hybrids, $[Ln(H_2O)_8]_2[Fe_4(H_2O)_8(thr)_2][B\text{-}\beta\text{-}SbW_9O_{33}]_2\cdot 22H_2O$ (Ln = Pr^{3+}, Nd^{3+}, Sm^{3+}, Eu^{3+}, Gd^{3+}, Dy^{3+}, Lu^{3+}; thr = threonine), which consisted of transition metal and lanthanide ions and amino acid components,[9q] as well as two classes of tetra-iron-substituted sandwich-type arsenotungstates with supporting Ln pendant groups, $[Ln(H_2O)_6][Fe_4(H_2O)_{10}(B\text{-}\beta\text{-}AsW_9O_{33})_2]^{3-}$ (Ln = La^{3+}, Pr^{3+}, Nd^{3+}, Sm^{3+}) and $[Ln(H_2O)_8]_2[Fe_4(H_2O)_8(L\text{-}thr)_2(B\text{-}\beta\text{-}AsW_9O_{33})_2]\cdot 20H_2O$ (Ln = La^{3+}, Pr^{3+}, Nd^{3+}, Sm^{3+}, Eu^{3+}, Gd^{3+}, Tb^{3+}, Dy^{3+}, Er^{3+}; L-thr = L-threonine).[9r] Clearly, the majority of these above-mentioned DFHPOMs are polyoxotungstates (PTs), and systematic explorations of 3d–4f heterometallic polyoxomolybdates (DFHPMs) remain underdeveloped, mainly because polyoxomolybdates (PMs) are not particularly stable in aqueous solution in comparison to PTs.[10] To date, only a relatively small number of DFHPMs have been reported.[11] In 2012, Li and coworkers reported two Anderson-type DFHPMs, $[\{CuTbL(H_2O)_3\}_2\{IMo_6O_{24}\}]Cl\cdot 2MeOH\cdot 8H_2O$ and $[\{CuTbL(H_2O)_2\}_2\{AlMo_6O_{18}(OH)_6\}_2]\cdot MeOH\cdot 10H_2O$ (L = *N*,*N*′-bis(3-methoxysalicylidene) ethylenediamine), which showed single-molecule magnet behavior.[11a] In the same year, the first cyanometalate-containing DFHPM $[\varepsilon\text{-}PMo_{12}O_{37}(OH)_3\{La(H_2O)_5(Fe(CN)_6)_{0.25}\}_4]\cdot 12H_2O$ was discovered by Ohkoshi and co-workers from a reaction between the mixed-valence ε-Keggin complex $[\varepsilon\text{-}PMo^V{}_8Mo^{VI}{}_4O_{36}(OH)_4\{La(H_2O)_4\}_4]^{5+}$ and hexacyanoferrate $[Fe^{II}(CN)_6]^{4-}$ under bench conditions at room temperature and ambient pressure.[11b] Therefore, the synthesis of innovative and functional DFHPMs it of urgent importance, although it remains a great challenge.

It is well-know that no saturated Keggin germanomolybdates (GM) that contain 3d–4f heterometallic groups have been reported. One reason for this deficit may be because the negative charge of the saturated Keggin GM polyoxoanion $[GeMo_{12}O_{40}]^{4-}$ is less than that of the lacunary Keggin GM polyoxoanion, $[GeMo_{11}O_{39}]^{8-}$ or $[GeMo_9O_{33}]^{8-}$, which makes the simultaneous combination of 3d-metal and 4f-metal cations with $[GeMo_{12}O_{40}]^{4-}$ polyoxoanions more difficult. However, it is also well-known that organic carboxylic acid ligands can act as negative-charge-compensation groups in the reaction system, because it can be deprotonated through coordination to transition metal and/or Ln ions,[12] which can effectively decrease the competition between 3d-/4f-metal cations and polyoxoanions. Furthermore, the introduction of organic carboxylic acid ligands has recently been put forward as an effective way to prevent precipitation, because organic carboxylic acid ligands can coordinate to Ln ions, thereby decreasing the highly oxophilic properties of the Ln ions.[13] Therefore, the selection of appropriate organic carboxylic acid ligands is vital for the preparation of DFHPOMs.

Based on these above-mentioned results, we recently began to investigate the preparation of new DFHPMs. Herein, we report our exploration of the reactions of GeO_2 and $(NH_4)_6(Mo_7O_{24})\cdot 4H_2O$ with $Ln(NO_3)_3\cdot 6H_2O$ and $CuCl_2\cdot 2H_2O$, with the participation of pyridyl carboxylic acid ligands under acidic reaction conditions, by using a strategy that combined in situ assembly and stepwise synthesis. Our approach was based on the following considerations: 1) acidic aqueous media can be beneficial for the formation of saturated Keggin polyoxoanions and can effectively decrease the precipitation of Ln^{3+} ions and afford crystalline compounds;[14] 2) Cu^{II} ions can adopt relatively diverse coordination configurations, with various linking modes, to generate unexpected structures;[9l,15] 3) based on the hard and soft acids and bases (HSAB) theory, 4f-metal ions behave as hard acids and prefer oxygen atoms to nitrogen donors, whereas 3d-metal ions are borderline acids and they have affinity for N-donors, as well as O-donors, which offers a high probability for the formation of new DFHPMs with pyridyl carboxylic acid ligands, which contain N- and O-coordination sites;[16] 4) the combined strategy of in situ assembly and stepwise synthesis is an effective way to construct DFHPMs, but it has seldom been used in the area of POMs synthesis.[17] Pleasingly, two types of unusual inorganic–organic hybrid Cu–Ln heterometal Keggin GMs, $[H_2INA]_2H_8[LnCu(INA)_4(H_2O)_6]_2[\alpha\text{-}GeMo_{12}O_{40}]_3\cdot 52H_2O$ (Ln = La^{3+} (**1**), Ce^{3+} (**2**), Pr^{3+} (**3**), Nd^{3+} (**4**), Sm^{3+} (**5**), Eu^{3+} (**6**); HINA = isonicotinic acid) and $(NH_4)[Ln(H_2O)_8][Cu(PA)_2]_2[\alpha\text{-}GeMo_{12}O_{40}]\cdot 10H_2O$ [Ln = Nd^{3+} (**7**), Sm^{3+} (**8**), Eu^{3+} (**9**); HPA = picolinic acid), were successfully synthesized by using this the strategy of combining in situ assembly and stepwise synthesis. Notably, the nature of the pyridine carboxylic acid ligand controlled the preference between the two structure types. Compounds **1**–**6** exhibited a trimeric structure that was defined by three Keggin-type $[\alpha\text{-}GeMo_{12}O_{40}]^{4-}$ polyoxoanions and two discrete $[LnCu(INA)_4(H_2O)_6]^+$ moieties, whilst compounds **7**–**9** exhibited an attractive 1D-chain architecture that was constructed from saturated $[\alpha\text{-}GeMo_{12}O_{40}]^{4-}$ polyoxoanions, pendent $[Cu(PA)_2]$ complexes, and bridging $\{[Cu(PA)_2][Ln(H_2O)_8]\}^{3+}$ heterometallic groups. Furthermore, the adsorption properties of compounds **3** and **8** have also been intensively studied.

2. Results and Discussion

2.1. Synthesis

Over the past few years, there has been tremendous development in the field of DFHPOMs;[5a–c,8–11] however, corresponding reports on DFHPMs are very limited. To the best of our knowledge, no 3d–4f heterometallic germanomolybdates (DFHGMs) have been reported to date, which offers us a wonderful opportunity to develop this field. Thus, we chose a system that contained an in-situ-formed $[\alpha\text{-}GeMo_{12}O_{40}]^{4-}$ polyoxoanion, Ln^{3+} and Cu^{2+} cations, and pyridyl carboxylic acid ligands to prepare neoteric DFHGMs. Herein, we utilized the strategy of

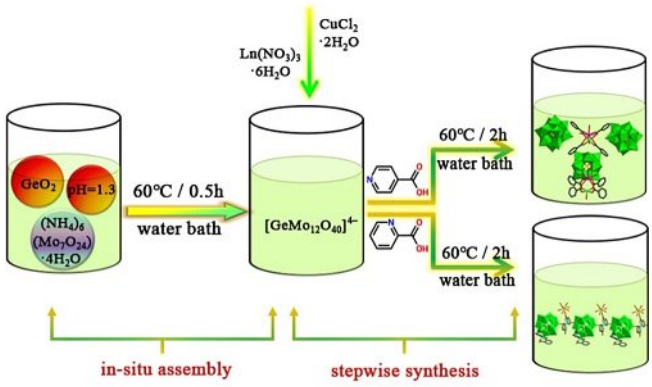

Scheme 1. Schematic representation of our preparation of compounds **1**–**9** through a combination of in situ assembly and stepwise synthesis.

combining in situ assembly with stepwise synthesis (Scheme 1).

Firstly, the reaction between $(NH_4)_6(Mo_7O_{24})\cdot 4H_2O$ and GeO_2 in acidic solution gave rise to the Keggin-type $[\alpha\text{-}GeMo_{12}O_{40}]^{4-}$ polyoxoanion, and the successive addition of Cu^{2+} ions, HINA or HPA, and Ln^{3+} ions led to the expected DFHGMs. By using this strategy, two new series of DFHGMs were synthesized under similar conditions. Our results indicated that the internal nature of the Cu^{2+} ions, Ln^{3+} ions, and the choice of HINA or HPA played a crucial role in the formation of these compounds. Notably, the diverse coordination modes of HINA or HPA, which contained both N- and O-coordination sites, had a crucial influence on the final structures of the DFHGMs: 1) the carboxylate groups could be deprotonated, which tended to increase the coordinating ability of HINA or HPA, and decrease the competition in the reaction system; 2) the carboxylate groups could rotate in a limited fashion, and so may connect metal ions in different directions, thereby resulting in rich coordination modes; 3) the pyridine rings not only provide N-donor atoms, but also rigidity, which help to generate crystalline products;[18] 4) in the absence of HINA or HPA, the desired crystals were not obtained.

Secondly, parallel experiments indicated that the use of Ln^{3+} ions was pivotal for the creation of the desired compounds: when La^{3+}–Eu^{3+} ions and HINA were used, compounds **1**–**6** were obtained, but, when Gd^{3+}–Yb^{3+} were used, no crystals of sufficient quality were obtained. When Nd^{3+}–Eu^{3+} cations and HPA were used, compounds **7**–**9** were obtained. Furthermore, we also found that the synthesis of these compounds rested upon the choice of the transition metal ion. If the Cu^{2+} ion was replaced by Co^{2+}, Ni^{2+}, or Fe^{3+} ions under similar conditions, the expected compounds were not obtained, primarily because the rich coordination geometries and the Jahn–Teller effect of Cu^{2+} ions played a key role in the formation of these compounds. We encountered similar results in our previous studies on DFHPTs.[9l] Finally, the pH value of the reaction system was very important for the preparation of compounds **1**–**9**. We found that compounds **1**–**6** could be obtained within the range pH = 1.2–2.1, and the highest yields were obtained at pH 1.3. Compounds **7**–**9** could be obtained within the range pH = 0.8–1.5, and the highest yields were obtained at pH 1.0. Apparently, the type of organic ligand was also vital for the creation of the different structural dimensions in compounds **1**–**9**. The further exploitation of DFHPMs is still a severe challenge for us, and our subsequent work to develop new Keggin-type DFHPM materials with potential applications is along these lines.

2.2. Structural Description

The conformity between the PXRD spectra of compounds **1**–**9** and their simulated XRD spectra based on single-crystal structure determination showed that the samples of these compounds were highly pure (see the Supporting Information, Figure S1). The crystal data and structural refinements of compounds **1**–**9** are listed in Table 1 and Table 2.

The crystal structures of compounds **1**–**9** each contained a plenary Keggin $[\alpha\text{-}GeMo_{12}O_{40}]^{4-}$ polyoxoanion. This $[\alpha\text{-}GeMo_{12}O_{40}]^{4-}$ polyoxoanion (the polyoxoanion in compound **8** is discussed herein as an example) is a common α-Keggin configuration and was constructed from a central $\{GeO_4\}$ tetrahedra that was connected to 12 $\{MoO_6\}$ octahedra in edge-sharing or vertex-sharing fashions (Figure 1 a). The $[\alpha\text{-}GeMo_{12}O_{40}]^{4-}$ polyoxoanion could also be described as follows: a central $\{GeO_4\}$ tetrahedron (Figure 1 b) was surrounded by four vertex-sharing $\{Mo_3O_{13}\}$ trimetal clusters (Figure 1 c), and each $\{Mo_3O_{13}\}$ group was comprised of three triangular-arranged $\{MoO_6\}$ fragments in an edge-sharing mode. Moreover, atoms Mo1, Mo3, and Mo5; atoms Mo2, Mo7, and Mo10; atoms Mo4, Mo11, and Mo12; and atoms Mo6, Mo8, Mo9 were each joined to the Ge center, thereby resulting in the formation of four $\{GeMo_3\}$ trigonal pyramids. These four trigonal pyramids surrounded the center of the $\{GeO_4\}$ tetrahedron (Figure 1 d). Moreover, three molybdenum atoms in each $\{Mo_3O_{13}\}$ cluster

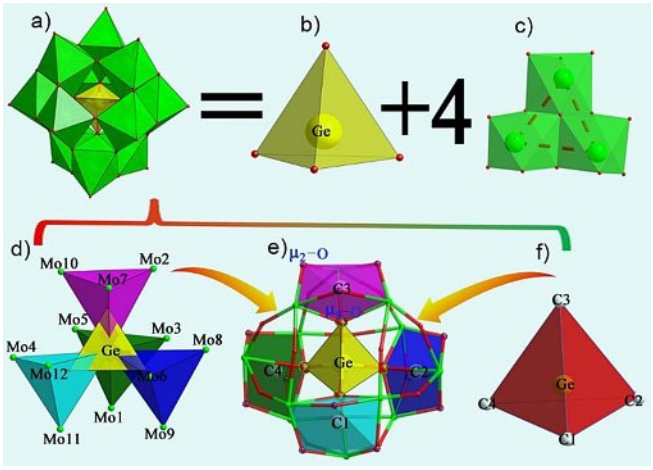

Figure 1. a–c) Structures of the $[GeMo_{12}O_{40}]^{4-}$ polyoxoanion in compound **8** (a), the $\{GeO_4\}$ tetrahedron (b), and the edge-sharing $\{Mo_3O_{13}\}$ trimetal cluster (c). d) The central $\{GeO_4\}$ tetrahedron is surrounded by four $\{GeMo_3\}$ trigonal pyramids in the $[\alpha\text{-}GeMo_{12}O_{40}]^{4-}$ polyoxoanion. e) Four cubane-like structures comprise the $[\alpha\text{-}GeMo_{12}O_{40}]^{4-}$ polyoxoanion. f) The {GeC1C2C3C4} atoms adopt a regular tetrahedral configuration.

Table 1. Crystallographic data and structure refinements for compounds **1–6**.

	1	2	3	4	5	6
empirical formula	$C_{60}H_{180}Cu_2Ge_3La_2Mo_{36}N_{10}O_{204}$	$C_{60}H_{180}Cu_2Ge_3Ce_2Mo_{36}N_{10}O_{204}$	$C_{60}H_{180}Cu_2Ge_3Pr_2Mo_{36}N_{10}O_{204}$	$C_{60}H_{180}Cu_2Ge_3Nd_2Mo_{36}N_{10}O_{204}$	$C_{60}H_{180}Cu_2Ge_3Sm_2Mo_{36}N_{10}O_{204}$	$C_{60}H_{180}Cu_2Ge_3Eu_2Mo_{36}N_{10}O_{204}$
formula weight	8382.65	8385.07	8386.65	8393.31	8405.53	8408.75
crystal system	tetragonal	tetragonal	tetragonal	tetragonal	tetragonal	tetragonal
space group	*P*4(2)/mnm	*P*4(2)/mnm	*P*4(2)/mnm	*P*4(2)/mnm	*P*4(2)/mnm	*P*4(2)/mnm
a [Å]	25.7680(8)	25.9624(16)	26.0465(5)	25.7873(10)	26.0326(6)	26.0525(5)
b [Å]	25.7680(8)	25.9624(16)	26.0465(5)	25.7873(10)	26.0326(6)	26.0525(5)
c [Å]	32.706(2)	32.733(4)	32.8176(13)	32.672(3)	32.6428(15)	32.6338(13)
α [°]	90	90	90	90	90	90
β [°]	90	90	90	90	90	90
γ [°]	90	90	90	90	90	90
V [Å^{-3}]	21 716.1(16)	22 064(4)	22 264.1(11)	21 726(2)	22 121.9(12)	22 149.6(11)
Z	4	4	4	4	4	4
μ [mm^{-1}]	3.112	3.088	3.089	3.195	3.199	3.231
F(000)	16 088	16 096	16 104	16 112	16 128	16 136
T [K]	296(2)	296(2)	296(2)	296(2)	296(2)	296(2)
limiting indices	$-19 \le h \le 30$ $-29 \le k \le 30$ $-38 \le l \le 38$	$-30 \le h \le 19$ $-30 \le k \le 29$ $-37 \le l \le 38$	$-26 \le h \le 30$ $-30 \le k \le 30$ $-30 \le l \le 39$	$-30 \le h \le 30$ $-19 \le k \le 30$ $-37 \le l \le 38$	$-27 \le h \le 30$ $-30 \le k \le 28$ $-27 \le l \le 38$	$-30 \le h \le 28$ $-30 \le k \le 27$ $-28 \le l \le 38$
total reflns	108 649	112 131	111 582	106 759	110 221	111 176
unique reflns	9987	10 238	10 229	9798	10 108	10 173
R_{int}	0.0588	0.0737	0.0722	0.1114	0.0739	0.1263
data/restrains/parameters	9987/4/520	10 238/10/563	10 229/4/556	9798/5/497	10 108/5/488	10 173/6/490
GOF on F^2	1.093	1.073	1.096	1.089	1.097	1.103
R [$I > 2\sigma(I)$]	*R*1 = 0.1011 *wR*2 = 0.2883	*R*1 = 0.0984 *wR*2 = 0.2844	*R*1 = 0.0911 *wR*2 = 0.2703	*R*1 = 0.0948 *wR*2 = 0.2679	*R*1 = 0.0932 *wR*2 = 0.2706	*R*1 = 0.0961 *wR*2 = 0.2779
R (all data)	*R*1 = 0.1309 *wR*2 = 0.3184	*R*1 = 0.1383 *wR*2 = 0.3180	*R*1 = 0.1262 *wR*2 = 0.3049	*R*1 = 0.1496 *wR*2 = 0.3106	*R*1 = 0.1332 *wR*2 = 0.3063	*R*1 = 0.1604 *wR*2 = 0.3237

Table 2. Crystallographic data and structure refinements for compounds **7–9**.

	7	8	9
empirical formula	$C_{24}H_{57}Cu_2GeMo_{12}N_5NdO_{66}$	$C_{24}H_{57}Cu_2GeMo_{12}N_5SmO_{66}$	$C_{24}H_{57}Cu_2GeMo_{12}N_5EuO_{66}$
formula weight	2966.94	2973.05	2974.66
crystal system	triclinic	triclinic	triclinic
space group	$P\bar{1}$	$P\bar{1}$	$P\bar{1}$
a [Å]	13.184(4)	13.1064(5)	13.1157(9)
b [Å]	13.948(4)	13.8620(5)	13.8652(9)
c [Å]	20.748(5)	20.6990(8)	20.7053(13)
α [°]	84.063(4)	84.1920(10)	84.1660(10)
β [°]	76.737(4)	76.6540(10)	76.9910(10)
γ [°]	86.707(4)	86.7620(10)	86.7100(10)
V [Å^{-3}]	3691.4(18)	3638.1(2)	3647.3(4)
Z	2	2	2
μ [mm^{-1}]	3.738	3.886	3.931
F(000)	2835	2840	2842
T [K]	296(2)	296(2)	296(2)
limiting indices	$-15 \le h \le 15$ $-16 \le k \le 16$ $-22 \le l \le 24$	$-15 \le h \le 15$ $-16 \le k \le 14$ $-24 \le l \le 24$	$-15 \le h \le 14$ $-7 \le k \le 16$ $-23 \le l \le 24$
total reflns	18 741	18 648	18 643
unique reflns	12 921	12 732	12 768
R_{int}	0.0183	0.0160	0.0247
data/restrains/parameters	12 921/1/978	12 732/1/977	12 768/0/981
GOF on F^2	1.077	1.037	1.032
R [$I > 2\sigma(I)$]	*R*1 = 0.0315 *wR*2 = 0.0916	*R*1 = 0.0306 *wR*2 = 0.0976	*R*1 = 0.0359 *wR*2 = 0.1018
R (all data)	*R*1 = 0.0350 *wR*2 = 0.0958	*R*1 = 0.0355 *wR*2 = 0.1044	*R*1 = 0.0409 *wR*2 = 0.1046

formed a cubane-like configuration through three μ_2-O atoms and one μ_4-O atom from the Mo_3O_{13} cluster (Figure 1e). Furthermore, we also observed that the centers (displayed as C1, C2, C3, C4) of four cubane-like configurations and the Ge atom formed a {GeC1C2C3C4} regular tetrahedral configuration (Figure 1f).

Compounds **1**–**6** belong to the tetragonal space group *P*4(2)/*mnm*, whereas compounds **7**–**9** crystallize in the triclinic space group $P\bar{1}$. As a consequence, the structures of compounds **2** and **8** are shown herein as representative examples. As shown in Figure 2a, compound **2** adopted an isolated structure that could be perceived as an aggregation of discrete ionic units. Its basic molecular unit consisted of three discrete classical Keggin-type heteropolymolybdate $[\alpha\text{-}GeMo_{12}O_{40}]^{4-}$ polyoxoanions (Figure 2b), two peculiar inorganic–organic hybrid dimeric Cu–Ce bimetallic $[CeCu(INA)_4(H_2O)_6]^+$ moieties (Figure 2c), two protonated HINA ligands, eight free H^+ cations, and 52 lattice water molecules. The oxidation states of the Ge, Cu, and Ce centers in compound **2** were certified by using bond valence sum (BVS) calculations and their oxidation states were +4, +2, and +3, respectively (see the Supporting Information, Table S1).[19] In the heteropolymolybdate $[\alpha\text{-}GeMo_{12}O_{40}]^{4-}$ anion, all of the Mo atoms adopted octahedral coordination geometries (Mo–O: 1.605(18)–2.405(19) Å, O–Mo–O: 48.2(8)–163.6(10)°). Furthermore, the Ge atom resided at the center of the $[\alpha\text{-}GeMo_{12}O_{40}]^{4-}$ polyoxoanion and was surrounded by eight disordered O atoms, each of which displayed half occupancy, thereby forming a cubic structure (Ge–O: 1.68(5)–1.768(18) Å, O–Ge–O: 66.9(11)–180(3)°; Figure 2d). This phenomenon is very common in Keggin structures, and has been reported by several groups.[20]

From the viewpoint of crystallography, in the Cu–Ce bimetallic $[CeCu(INA)_4(H_2O)_6]^+$ moieties, the $Cu1^{2+}$ and $Cu2^{2+}$ ions exhibited similar coordination geometries, whilst the $Ce1^{3+}$ and $Ce2^{3+}$ ions manifested similar coordination configurations. Therefore, only the $Cu1^{2+}$ and $Ce1^{3+}$ ions are described in detail herein. The $Cu1^{2+}$ ion was pentacoordinate, comprising four carboxy oxygen atoms from INA^- ligands and a water ligand in a square-pyramidal geometry (Figure 2e). The four carboxy oxygen atoms from the INA^- ligands (O39, O39A, O39B, and O39C) formed the four vertices of a square (O···O: 2.7 Å) and the $Cu1^{2+}$ ion was situated at its center (Cu–O: 1.9 Å). The O4W atom occupied the apical site of the square pyramid (Cu–O: 2.2 Å). Conversely, the $Ce1^{3+}$ ion was nonacoordinate, with a monocapped square-antiprism configuration that was constructed from nine O atoms from four INA^- ligands (La1–O: 2.473(11) Å) and five aqueous ligands (La1–O: 2.548(16)–2.585(17) Å; Figure 2f and the Supporting Information, Table S2). In the monocapped square antiprism of the $Ce1^{3+}$ ion, the O1W, O1WB, O3W, and O3WB group and the O40, O40A, O40B, and O40C group made up the two bottom planes of the square antiprism and their least-square standard deviations were 0.0438 Å and 0.0000 Å, respectively, whilst the separations between the $Ce1^{3+}$ cation and the two bottom planes were 0.8954 Å and 1.4182 Å, respectively. The O2W atom was located at the "cap" position, above one bottom plane that was constituted by the O1W, O1WB, O3W, and O3WB group, and the separation between the O2W atom and the bottom surface was 1.6646 Å. Attractively, in the bimetallic $[Ce1Cu1(INA)_4(H_2O)_6]^+$ moiety, the $Cu1^{2+}$ and $Ce1^{3+}$ ions were bridged by eight carboxy oxygen atoms from four INA^- ligands (O39, O39A, O39B, O39C, O40, O40A, O40B, and O40C), which formed a captivating "house-like" structure (Figure 2g). Two adjacent INA^- ligands in the bimetallic $[Ce1Cu1(INA)_4(H_2O)_6]^+$ moiety were approximately perpendicular to each other, thereby forming a cross-surface structure (Figure 2h). Undoubtedly, the INA^- ligands played a significant role in stabilizing the bimetallic $[CeCu(INA)_4(H_2O)_6]^+$ moiety, which may also demonstrate their huge potential in the construction of new DFHPOMs.

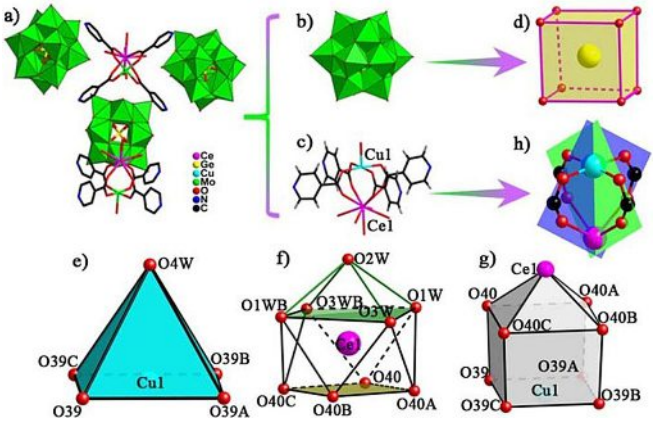

Figure 2. Structure of compound **2**: a) molecular unit; b) $[\alpha\text{-}GeMo_{12}O_{40}]^{4-}$ polyoxoanion; c) Cu–Ce bimetallic $[CeCu(INA)_4(H_2O)_6]^+$ moiety; d) cubic structure of the disordered $\{GeO_4\}$ group in the $[\alpha\text{-}GeMo_{12}O_{40}]^{4-}$ polyoxoanion; e) square-pyramidal geometry of the $Cu1^{2+}$ ion; f) monocapped square antiprismatic geometry of the $Ce1^{3+}$ ion; g) "house-like" structure of the $Cu1^{2+}$ and $Ce1^{3+}$ ions; and h) cross-surface structure in the $[CeCu(INA)_4(H_2O)_6]^+$ moiety. Atoms with the suffixes A, B, and C were generated by using the symmetry operation: A = *x*, *y*, 1−*z*; B = 1−*y*, 1−*x*, 1−*z*; C = 1−*y*, 1−*x*, *z*; W = water.

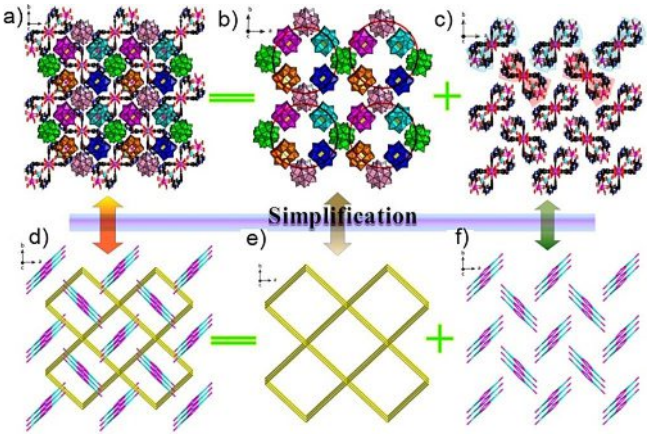

Figure 3. Packing of compound **2**: a) 3D packing, viewed along the *c* axis; b) $[\alpha\text{-}GeMo_{12}O_{40}]^{4-}$ polyoxoanions in the 3D packing; c) $[CeCu(INA)_4(H_2O)_6]^+$ moieties in the 3D packing; d) simplified 3D packing, viewed along the *c* axis; e) $[\alpha\text{-}GeMo_{12}O_{40}]^{4-}$ polyoxoanions in the simplified 3D packing; f) $[CeCu(INA)_4(H_2O)_6]^+$ moieties in the simplified 3D packing.

A representation of the 3D packing of compound **2** along the *c* axis is shown in Figure 3a. To understand the 3D packing of compound **2**, its packing structure was further divided into two subcategories: $[\alpha\text{-}GeMo_{12}O_{40}]^{4-}$ polyoxoanions and $[CeCu(INA)_4(H_2O)_6]^{+}$ moieties. As shown in Figure 3b, eight neighboring $[\alpha\text{-}GeMo_{12}O_{40}]^{4-}$ polyoxoanions formed a rhombic repeating unit. Closer examination revealed that neighboring $[\alpha\text{-}GeMo_{12}O_{40}]^{4-}$ polyoxoanions were arranged in different orientations, which not only decreased the steric hindrance as much as possible, but also enhanced the structural stability of compound **2**. In the *ab* plane, the rhombus repeating units were tidily arranged in an -AAA- fashion along the *a* or *b* axis. On the other hand, four neighboring $[CeCu(INA)_4(H_2O)_6]^{+}$ moieties formed a "bowknot-like" repeating unit, which were regularly arranged in a staggered fashion, thereby exhibiting an -ABAB- pattern along the *a* or *b* axis (Figure 3c). Furthermore, the 3D stacking arrangement of compound **2** and the $[CeCu(INA)_4(H_2O)_6]^{+}$ repeating units exhibited square-shaped stacking structures (see the Supporting Information, Figure S2). More interestingly, the 3D packing of compound **2**, with $[\alpha\text{-}GeMo_{12}O_{40}]^{4-}$ and $[CeCu(INA)_4(H_2O)_6]^{+}$ repeating units along the *c* axis, could be simplified as shown in Figure 3d–f. The $[\alpha\text{-}GeMo_{12}O_{40}]^{4-}$ units and $[CeCu(INA)_4(H_2O)_6]^{+}$ moieties were inlaid with each other (Figure 3d), which enhanced the structure stability of compound **2** to some extent.

The molecular fragment of compound **8** (Figure 4a) comprised a typical Keggin-type $[\alpha\text{-}GeMo_{12}O_{40}]^{4-}$ polyoxoanion (Figure 4b), a pendent $[Cu(PA)_2]$ complex (Figure 4c), a bridging $\{[Cu(PA)_2][Sm(H_2O)_8]\}^{3+}$ bimetallic subunit (Figure 4d), a NH_4^+ ion, and 12 lattice water molecules. Unlike compound **2**, the central $\{GeO_4\}$ group of the Keggin-type $[\alpha\text{-}GeMo_{12}O_{40}]^{4-}$ polyoxoanion in compound **8** adopted a tetrahedral geometry (Ge–O: 1.730(3)–1.741(4) Å; O–Ge–O: 108.84(18)–110.14(17)°; Figure 4e). Interestingly, two crystallographically unique Cu^{2+} ions ($Cu1^{2+}$ and $Cu2^{2+}$) in compound **8** revealed two types of coordination geometry. The $Cu2^{2+}$ ion in the pendant $[Cu(PA)_2]$ complex attached to the Keggin-type $[\alpha\text{-}GeMo_{12}O_{40}]^{4-}$ polyoxoanion through a bridging O31 atom and inhabited a severely contorted square-pyramidal configuration (Figure 4f), in which two N atoms (N3 and N4) and two O atoms (O42 and O43) from two PA^- ligands occupied the bottom plane (Cu–N: 1.971(5)–1.974(5) Å; Cu–O: 1.947(4)–1.961(4) Å) and the bridging O31 atom (Cu–O: 2.431(4) Å) was located at the apical position. The $Cu1^{2+}$ cation in the bridging $\{[Cu(PA)_2][Sm(H_2O)_8]\}^{3+}$ bimetallic subunit was embedded in an elongated octahedron (Figure 4g), in which the basal positions were occupied by two N atoms (N1 and N2) and two O atoms (O46 and O47) from two PA^- ligands (Cu–N: 1.947(5)–1.953(5) Å; Cu–O: 1.929(4)–1.932(4) Å) and the two axial positions were occupied by two oxygen atoms (O16 and O1#). The O16 atom was a terminal O atom from the $[\alpha\text{-}GeMo_{12}O_{40}]^{4-}$ polyoxoanion (Cu–O: 2.712(4) Å), whilst the O1# atom was a bridging O atom from the adjacent $[\alpha\text{-}GeMo_{12}O_{40}]^{4-}$ polyoxoanion (Cu–O: 3.095(4) Å). The crystallographically unique $Sm1^{3+}$ ion was bound to eight O atoms (O1W, O2W, O3W, O4W, O5W, O6W, O7W, O8W) from eight coordinated water molecules (Sm–O: 2.437(5)–2.523(4) Å), one carboxy O atom from the tridentate PA^- ligand (O45; Sm–O: 2.420(4) Å) and adopted a nonacoordinate monocapped square antiprismatic geometry (Figure 4h). Fascinatingly, in compound **8**, the PA^- ligands possessed two different coordination modes: 1) as a bidentate ligand to chelate a Cu^{2+} ion through a carboxy O atom and a pyridine N atom (Figure 4c and 4i); and 2) as a tridentate ligand to chelate a Cu^{2+} ion through a carboxy O atom and a pyridine N atom, in addition to connecting a Sm^{3+} ion by utilizing the remaining carboxy O atom (Figure 4j).

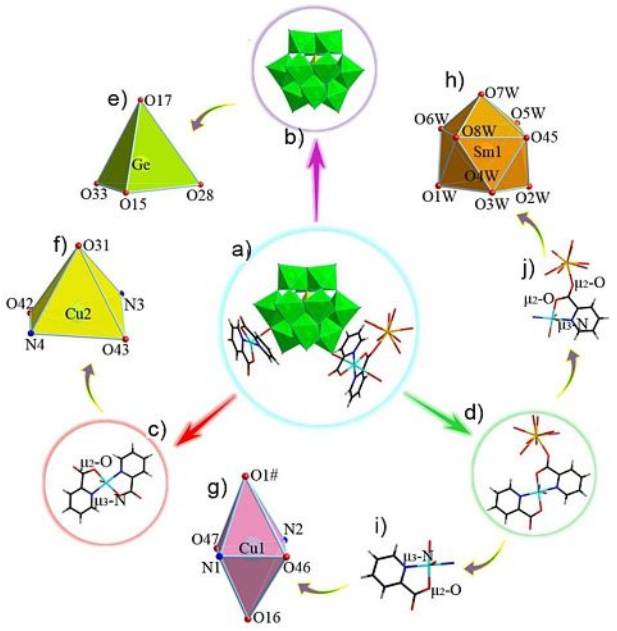

Figure 4. Structure of compound **8**: a) Fundamental structural unit; b) $[\alpha\text{-}GeMo_{12}O_{40}]^{4-}$ polyoxoanion; c) pendent $[Cu(PA)_2]$ complex; d) bridging $\{[Cu(PA)_2][Sm(H_2O)_8]\}^{3+}$ bimetallic subunit; e) tetrahedral geometry of the Ge atom in the $[\alpha\text{-}GeMo_{12}O_{40}]^{4-}$ polyoxoanion; f) severely distorted square-pyramid configuration of the $Cu2^{2+}$ ion; g) elongated octahedral configuration of the $Cu1^{2+}$ ion; h) mono-capped square antiprismatic geometry of the $Sm1^{3+}$ ion; i) bidentate PA^- ligand, which chelates a Cu^{2+} ion with a μ_2-O atom and a μ_3-N atom; and j) tridentate PA^- ligands, which chelate a Cu^{2+} ion and a Sm^{3+} ion with two μ_2-O atoms and a μ_3-N atom.

The most prominent structural trait of compound **8** is that neighboring molecular moieties are fused together through the bridging $\{[Cu1(PA)_2][Sm(H_2O)_8]\}^{3+}$ bimetallic subunit, which leads to the formation of beautiful 1D chains (Figure 5a). Notably, compound **8** is the first example of an infinite 1D chain that is made up of $[\alpha\text{-}GeMo_{12}O_{40}]^{4-}$ polyoxoanions and $\{[Cu1(PA)_2][Sm(H_2O)_8]\}^{3+}$ bimetallic linkers. Although abundant 1D chain POMs that are linked by transition metal or Ln cations have been reported,[9m,21] the simultaneous bridging of POMs by transition metal and Ln ions has not previously been encountered. Furthermore, the 2D packing arrangements in compound **8** were also investigated and, in the *ab* plane, the alignments in the 1D chain revealed an -AAA- pattern in the *a* direction (Figure 5b). However, in the *bc* plane, the 1D chains were stacked in a staggered fashion, with an -ABAB- mode along the *c* axis (Figures 5c,d), which may have contributed to decreasing the steric hindrance.

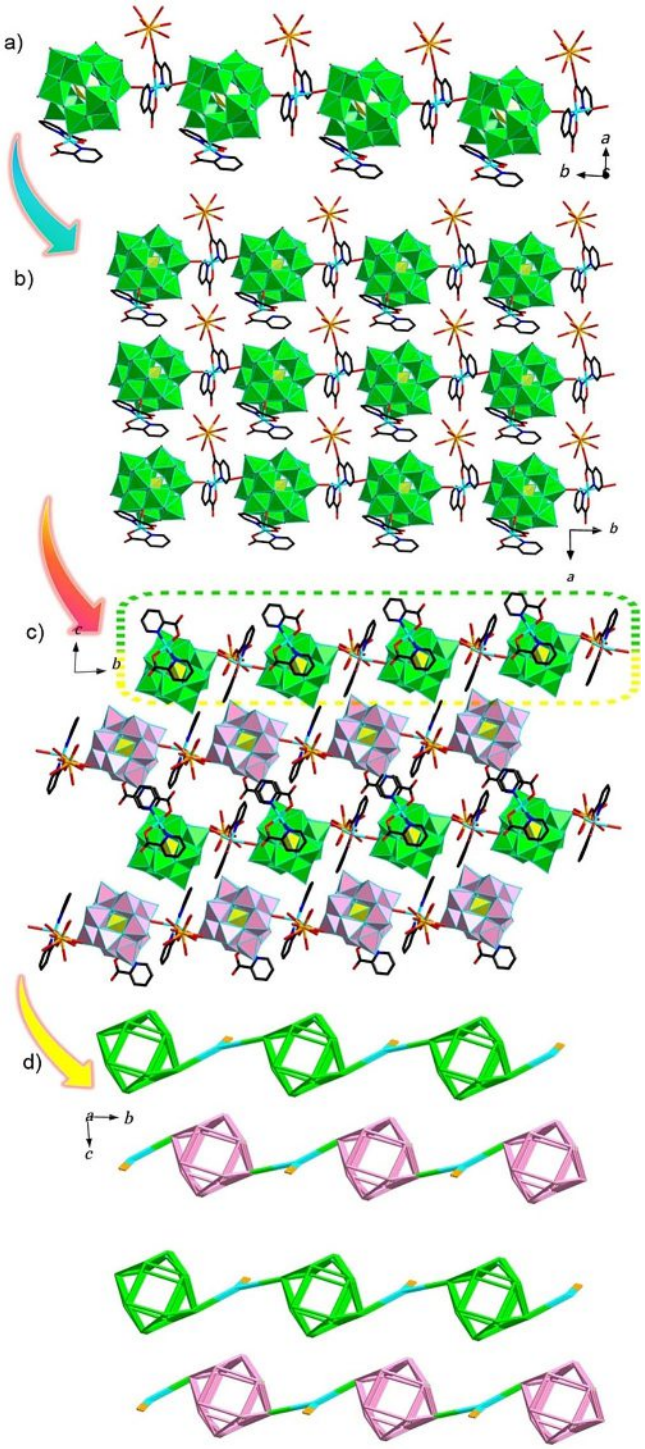

Figure 5. a) 1D chain of compound **8**, viewed along the *c* axis; b) 2D packing in the *ab* plane, which highlights the -AAA- alignment pattern of the 1D chains; c) 2D packing in the *bc* plane, which highlights the -ABAB- alignment pattern of the 1D chains; and d) simplified 2D packing in the *bc* plane.

The fundamental skeletons of compounds **1**–**9** all shared the classical Keggin-type $[\alpha\text{-}GeMo_{12}O_{40}]^{4-}$ polyoxoanions and Cu–Ln–organic subunits. However, there were two main differentiators between compounds **1**–**6** and compounds **7**–**9**: 1) in terms of their synthesis, two different bipyridyl carboxylic ligands (HINA and HPA) were used; and 2) in terms of their structures, compounds **1**–**6** adopted isolated structures, whereas compounds **7**–**9** adopted 1D-chain structures. Moreover, in compounds **1**–**6**, only the O atoms connected the Cu^{2+} and Ln^{3+} ions in the $[LnCu(INA)_4(H_2O)_6]^+$ moieties (Figures 2c and the Supporting Information, S3a), and the Cu^{2+} and Ln^{3+} ions were bridged by four INA^- ligands, thereby forming a "windmill-like" structure. Alternatively, in compounds **7**–**9**, the HPA ligands in the $\{[Cu(PA)_2][Ln(H_2O)_8]\}^{3+}$ group chelated to the Cu^{2+} and Ln^{3+} ions through N and O atoms, thereby giving rise to the five-membered-ringed structure (Figure 3d and the Supporting Information, S3b).

2.3. Thermogravimetric Analysis

To investigate the thermal stability of compounds **1**–**9**, thermogravimetric analysis (TGA) was performed under a nitrogen atmosphere from 25–1000 °C at a heating rate of 10 °C min^{-1}. The TGA curves revealed that the weight-loss processes for compounds **1**–**9** could each be divided into two steps (see the Supporting Information, Figure S4). The thermal decomposition processes for compounds **1**–**6** were quite similar to one another. The first weight losses of 13.44% (calcd 13.74%), 12.94% (calcd 13.74%), 12.91% (calcd 13.74%), 13.59% (calcd 13.73%), 13.44% (calcd 13.71%), and 12.94% (calcd 13.70%) for compounds **1**–**6**, respectively, were observed between 25 and 300 °C, which corresponded to evaporation of the 52 lattice water molecules and 12 coordinated water molecules. Then, upon further heating, second weight losses of 23.37% (calcd 23.47%), 23.06% (calcd 23.47%), 23.89% (calcd 23.46%), 23.22% (calcd 23.44%), 22.55% (calcd 23.41%), and 22.61% (calcd 23.40%) for compounds **1**–**6**, respectively, were observed between 300 and 1000 °C, which were attributed to the dehydration of two protons, the release of 10 HINA ligands, and the sublimation of five MoO_3 molecules, which stemmed from decomposition of the polyoxoanions. In the case of compounds **7**–**9**, the first weight losses of 13.01% (calcd 12.56%), 12.47% (calcd 12.53%), and 12.46% (calcd 12.53%), respectively, occurred between 25 and 300 °C, which were assigned to the evaporation of 12 lattice water molecules, eight coordinated water molecules, and one NH_3 molecule. Second weight losses of 27.15% (calcd 25.98%), 27.01% (calcd 25.93%), and 26.75% (calcd 25.91%) for compounds **7**–**9**, respectively, were observed between 300 and 1000 °C, which corresponded to the removal of four HPA ligands and the sublimation of two MoO_3 molecules, which stemmed from decomposition of the polyoxoanions.

2.4. Dye Adsorption and Selective Adsorption

It is well known that, on one hand, organic dyes have a wide range of applications, such as in textiles, plastics, leather, and paper,[22] whilst, on the other hand, they also exhibit persistent toxicity and present a carcinogenic risk that can seriously threaten living environments, human health, and aquatic life.[23] Therefore, a large number of methods have been proposed and used to minimize the effect of dye wastewater on the environment,[24] among which the adsorption method is

one of the most effective approaches for coping with organic dye pollution, because of its effectiveness, efficiency, and commercial value.[22a,25] In recent years, it has been shown that some organic–inorganic hybrid POM materials can also function as effective photocatalysts for the degradation of hazardous dyes in water.[26] In contrast, reports on the use of POM-based hybrid materials as highly efficient adsorbents for the removal of hazardous dyes remain relatively rare.[27] As a consequence, the search for materials with efficient dye-adsorption ability remains a challenge. Therefore, herein, we systematically explored the dye-capture behavior of compounds **3** and **8** as representative examples of this class of compound. The effects of crystal size, stirring conditions, dye category, dye concentration, and adsorbent dosage on the adsorption properties of compounds **3** and **8** were investigated under natural light at room temperature. A suitable amount of the prepared sample was placed in a 40 mL solution of the dye at a known concentration. After predetermined time intervals, an aliquot of the dye solution (3 mL) was removed and subjected to centrifugal separation at 10000 rpm for 2 min. The dye concentration was monitored by using UV/Vis absorption spectroscopy.

2.5. Effects of Crystal Size and Stirring Conditions

The effects of crystal size and stirring conditions on the adsorption behavior of compounds **3** and **8** for cationic dye rhodamine B (RhB) were examined under the following conditions: 1) the as-synthesized crystals were immersed in RhB solution without stirring (Figure 6a,c); 2) the powdered crystals were

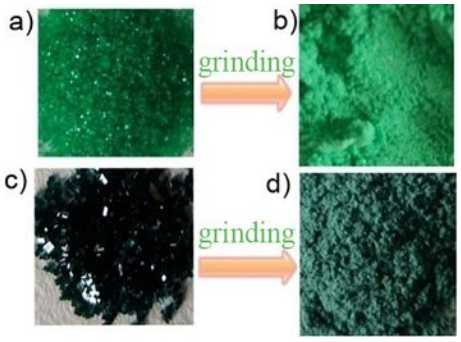

Figure 6. a) Synthetic crystals of compound **3**; b) powdered crystals of compound **3**; c) synthetic crystals of compound **8**; and d) powdered crystals of compound **8**.

immersed in RhB solution without stirring (Figure 6b,d); 3) the as-synthesized crystals were immersed in RhB solution with stirring (500 rpm); and 4) powdered crystals were immersed in RhB solution with stirring (500 rpm). The same initial conditions (5 mg sample, 10 mg L^{-1}, 40 mL solution of RhB in water) were employed for all of the tests. Moreover, for comparison, a dye-adsorption experiment of the RhB solution (10 mg L^{-1}, 40 mL) without any adsorbent was also performed. In this reaction, the adsorption ability of RhB was quantified by measuring the intensity-decay rate of its characteristic absorption band at $\lambda \approx 554$ nm. In addition, the adsorption ability of the dye could be quantified by its removal efficiency ($R.$), according to $R. = (C_0-C_t)/C_0 = (A_0-A_t)/A_0$, in which C_0 and C_t (in mg L^{-1}) denote the initial concentration of the dye and the residual concentration after adsorption for time t, respectively, and A_0 and A_t denote the absorbance of the dye before and after the adsorption, respectively.

As shown in Figure 7a, the UV/Vis spectrum of RhB without any adsorbent exhibited no clear changes, even after exposure to natural light for one day at room temperature, which indicated that RhB was unaffected under these conditions. In addition, the adsorption equilibria for compounds **3** and **8** could be completed within about 9 min (Figure 7b–e, g–i), except for the test in which as-synthesized crystals of compound **8** were used without stirring, for which the equilibrium time was about 21 min (Figure 7f). In the presence of compound **3**, the removal efficiencies of RhB were up to 72.8%, 68.1%, 73.0%, and 71.1% within 9 min for the four conditions tested (Figure 7b–e). Furthermore, with compound **8**, the removal efficiency of RhB reached 68.1% within 21 min and 72.9%, 76.8%, and 77.9% within 9 min for the four conditions tested (Figure 7b–i).

2.6. Effect of the Dye Category

We postulate that the absorption properties of as-synthesized crystals **3** and **8** towards cationic dye RhB may be owing to electrostatic attraction interactions between negatively charged surfaces of as-synthesized crystals **3** and **8** and positively charged RhB molecules. To confirm this conjecture, we also performed comparative adsorption experiments with another cationic dye, methylene blue (MB; 10 mg L^{-1}), as well as two anionic dyes, azophloxine (Apo; 10 mg L^{-1}) and methyl orange (MO; 20 mg L^{-1}), as dye pollutants under similar conditions (see the Supporting Information, Figure S5).

As shown in Figure 8a,b, in the presence of as-synthesized crystals of compounds **3** and **8**, the absorption intensity of the characteristic band of MB clearly decreased when the adsorption time increased. The removal efficiency of MB was approximately 81.0% and 78.8% after 9 min in the presence of as-synthesized crystals of compounds **3** and **8**, respectively. In contrast, the adsorption ability of as-synthesized crystals of compounds **3** and **8** towards anionic dyes Apo and MO was negligible (Figure 8c–f). Based on these results, as-synthesized crystals of compounds **3** and **8** clearly showed better adsorption properties for cationic dyes RhB and MB than for anionic dyes MO and Apo, possibly because the oxo-enriched and highly negatively charged surfaces of the polyoxoanions in compounds **3** and **8** could form stronger electrostatic interactions with cationic dyes.[28] At the same time, the removal efficiency for MB was higher than that for RhB, which may be owing to the size of RhB, which led to higher steric hindrance between the POM fragments and the RhB components.[29] Based on these findings, we selected MB as a representative dye to explore the dye adsorption and adsorption selectivity of these compounds.

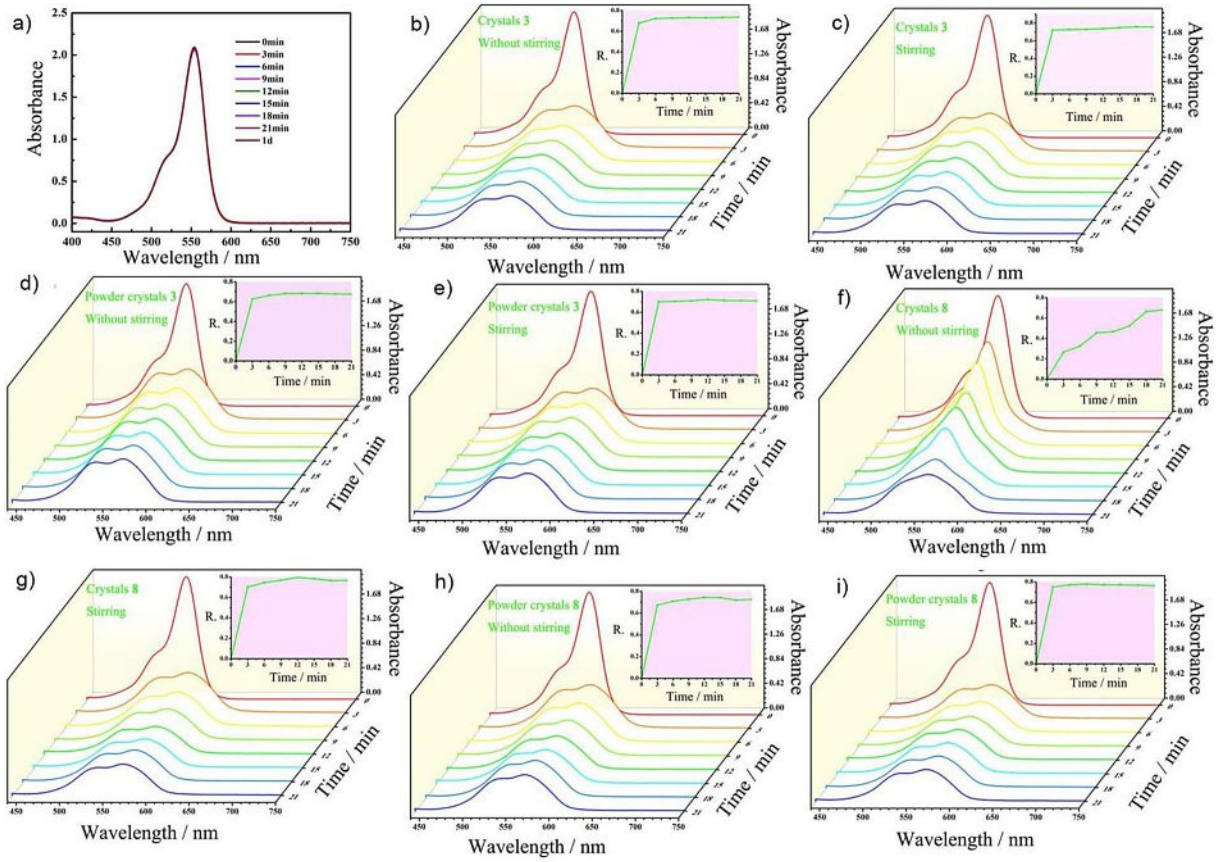

Figure 7. Changes in the UV/Vis absorption spectra of solutions of RhB after various adsorption times: a) without any adsorbent; b) in the presence of crystals of compound **3** (5 mg) without stirring; c) in the presence of crystals of compound **3** (5 mg) with stirring; d) in the presence of powdered crystals of compound **3** (5 mg) without stirring; e) in the presence of powdered crystals of compound **3** (5 mg) with stirring; f) in the presence of crystals of compound **8** (5 mg) without stirring; g) in the presence of crystals of compound **8** (5 mg) with stirring; h) in the presence of powdered crystals of compound **8** (5 mg) without stirring; and i) in the presence of powdered crystals of compound **8** (5 mg) with stirring. Inset: plot of the removal efficiency (*R.*) of RhB versus reaction time.

2.7. Effect of Dye Concentration

Adsorption ability is heavily influenced by the dye concentration.[30] To determine the adsorption ability of as-synthesized crystals of compounds **3** and **8** for MB, UV/Vis spectra of various solutions of MB were recorded and a linear best-fit was established for a plot of absorbance versus concentration (C_0; Figure 9). Then, the degree of adsorption of MB on as-synthesized crystals of compounds **3** and **8** was calculated by using the equation: $Q_t=(C_0-C_t)V/m$,[31] in which C_0 (in mg L^{-1}) and C_t (in mg L^{-1}) denote the concentrations of aqueous solutions of MB at the starting time ($t=0$) and after the equilibrium time (t, in min), respectively; V (in L) denotes the volume of the aqueous solution of MB; and m (in g) denotes the mass of compound **3** or **8**. During the adsorption process, the as-synthesized crystals of compound **3** or **8** (5 mg) were used to remove MB in various concentrations from 10–40 mg L^{-1}.

As shown in Figure 10 and the Supporting Information, S6, on enhancing the starting concentration of MB from 10 mg L^{-1} to 40 mg L^{-1}, the removal efficiency was slightly elevated to 79.1%, 87.3%, 89.3%, and 95.7% (for **3**) and to 90.5%, 92.7%, 97.0%, and 97.1% (for **8**) after 60 min. Interestingly, the higher the starting concentration, the longer the system took to reach equilibrium. Furthermore, the adsorption ability of as-synthesized crystals of compounds **3** and **8** towards MB gradually increased during the initial stage and thereafter it proceeded slowly before ultimately reaching equilibrium. The equilibrium adsorption ability (Q_e) increases from 5.65 mg g^{-1} to 25.64 mg g^{-1} (for **3**) and from 6.46 mg g^{-1} to 26.01 mg g^{-1} (for **8**) on increasing the starting concentration of MB from 10 mg L^{-1} to 40 mg L^{-1}. We found that most of the unoccupied surface sites for as-synthesized crystals of compounds **3** and **8** were available for adsorption during the initial period and the concentration of MB was high during this stage, which provided a strong driving force for breaking through the mass-transfer resistance of the dye between the water and solid phases.[32] Therefore, a higher starting concentration of MB tended to promote the adsorption procedure.[32b] However, during the adsorption process, the number of available surface sites became less and less, because of repulsive forces between the MB molecules; therefore, the adsorption of MB reached equilibrium in the final stage.[32c]

Moreover, by raising the concentration of MB, the driving force increased, thereby resulting in higher adsorption ability. Furthermore, the adsorption ability was 164.77 mg g^{-1} (for **3**)

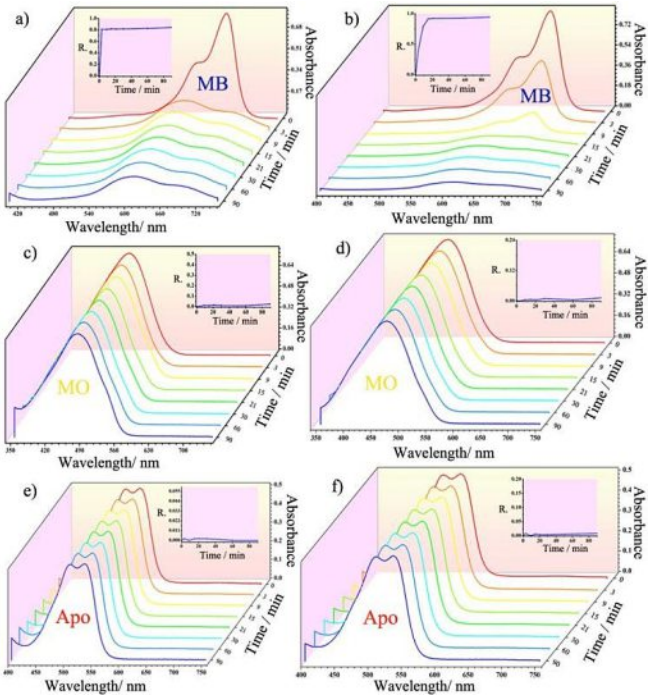

Figure 8. Changes in the UV/Vis absorption spectra for different dye solutions after different adsorption times: a) as-synthesized crystals of compound **3** (5 mg) in a solution of MB; b) as-synthesized crystals of compound **8** (5 mg) in a solution of MB; c) as-synthesized crystals of compound **3** (5 mg) in a solution of MO; d) as-synthesized crystals of compound **8** (5 mg) in a solution of MO; e) as-synthesized crystals of compound **3** (5 mg) in a solution of Apo; and f) as-synthesized crystals of compound **8** (5 mg) in a solution of Apo. Inset: plot of the removal efficiency (*R.*) of the different dyes versus reaction time.

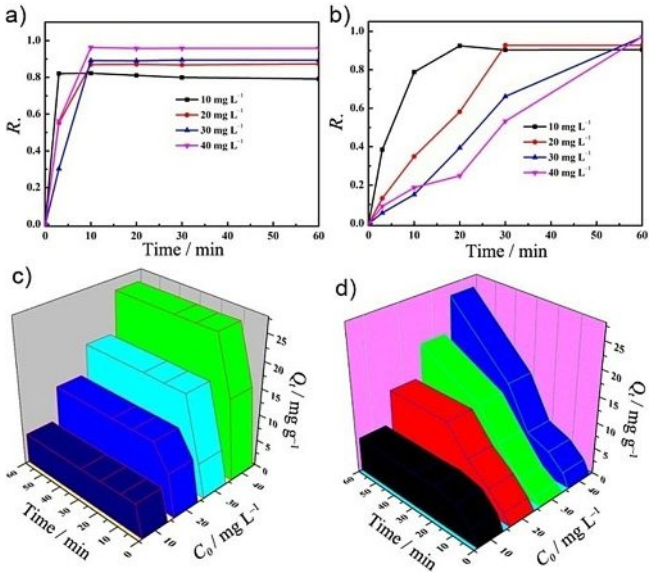

Figure 10. a, b) Effect of dye concentration on the removal efficiency (*R.*) of MB for as-synthesized crystals of compounds **3** (a) and **8** (b). c, d) Effect of dye concentration on the adsorption ability of MB for as-synthesized crystals of compounds **3** (c) and **8** (d).

and 96.29 mg g^{-1} (for **8**) when as-synthesized crystals of compounds **3** and **8** (5 mg) were immersed in MB solution (100 mL, 100 mg L^{-1}) for 240 min. Compared to previous reports for POMs or other adsorbents,[32c,33] compounds **3** and **8** exhibited good adsorption ability for MB (see the Supporting Information, Table S3). For example, the corresponding adsorption ability for MB of activated carbon is 135 mg g^{-1},[33h] carbon nanotubes is 35.4 mg g^{-1},[33e] $H_6P_2W_{18}O_{62}$/MOF-5 is 51.81 mg g^{-1},[33c] and $H_3PW_{12}O_{40}$@Mn^{III}–porphyrin is 10.5 mg g^{-1}.[33d] Furthermore, compared with previously reported POMs for dye sorption,[33c,d] as-synthesized crystals of compounds **3** and **8** didn't require an activation process. Thus, as-synthesized crystals of compounds **3** and **8** may be promising adsorbents for the disposing of harmful organic contaminants in dye wastewater.

2.8. Effect of Adsorbent Dosage

The dosage of an adsorbent is a pivotal parameter that must be prudentially adjusted during the course of wastewater treatment. To determine the optimal amount of adsorbent required to maximize the interactions between MB molecules and the adsorption sites on the adsorbent in solution, we measured the effect of the adsorbent dosage of as-synthesized crystals of compounds **3** and **8** (2–20 mg) on the removal of MB dye (40 mL, 20 mg L^{-1}; Figure 11 and the Supporting Information, S7). Our results showed that the time required to achieve adsorption equilibrium for the as-synthesized crystals of compounds **3** and **8** with MB notably shortened from 20 min to 3 min (for **3**) and from 60 min to 20 min (for **8**) when the

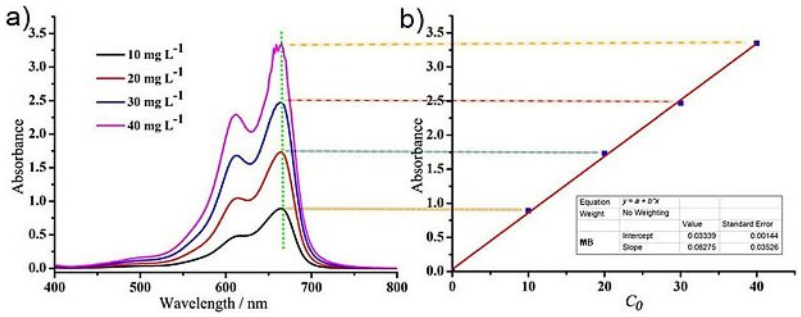

Figure 9. a) UV/Vis spectra of aqueous solutions of different concentrations of MB dye; b) plot of absorption intensity (blue dots) versus the concentration of MB dye. The solid red line denotes the best linear fit.

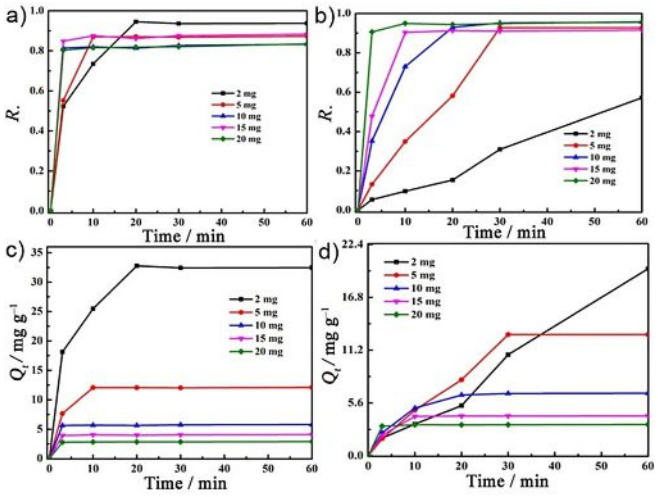

Figure 11. a, b) Effect of the adsorbent dosage of compounds **3** (a) and **8** (b) on the removal efficiency (*R.*) of MB. c, d) Effect of the adsorbent dosage of compounds **3** (c) and **8** (d) on the adsorption ability of MB.

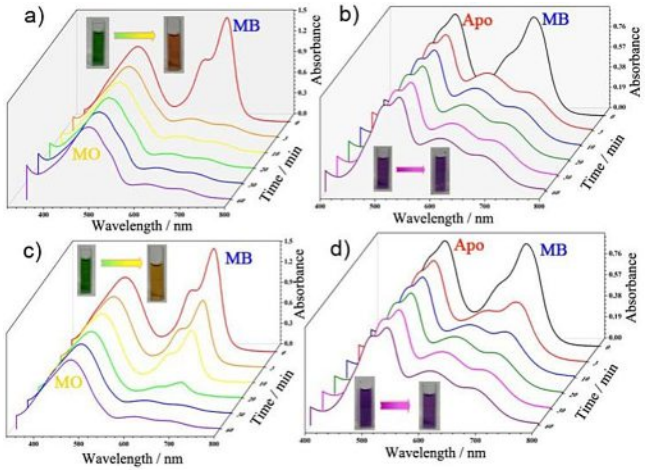

Figure 12. a, b) Selective adsorption ability of compound **3** in binary mixtures of MB/MO (a) and MB/Apo (b). c, d) Selective adsorption ability of compound **8** in binary mixtures of MB/MO (c) and MB/Apo (d). Insets: photographs of the mixed dyes before the start of the experiment and after 60 min.

adsorbent dosage increased from 2 mg to 10 mg, owing to an increase in the number of available adsorption sites on the adsorbent surface.[32a,34] Further increasing the adsorbent dosage from 10 mg to 20 mg didn't significantly increase the degree of dye removal. Moreover, the equilibrium adsorption ability (Q_e) of as-synthesized crystals of compounds **3** and **8** decreased from 32.48 mg g^{-1} to 2.89 mg g^{-1} (for **3**) and from 19.82 mg g^{-1} to 3.32 mg g^{-1} (for **8**) when the adsorbent dosage was increased from 2 mg to 20 mg. At low adsorbent dosages, the surface sites were completely exposed for adsorption and quickly reached saturation, thereby leading to larger adsorption ability. However, the number of available higher-energy sites at higher adsorbent dosages decreased, because a larger number of lower-energy sites had been occupied, thereby resulting in poorer adsorption ability.[35]

2.9. Selective Adsorption of Mixed Dyes

An excellent adsorbent not only requires good adsorption ability, but also must display outstanding selectivity. The ingredients in a dye are very complicated, often including disparate kinds of chromophores (such as –N=N–, $-SO_3$, –N=O, and –NH groups).[32c] Thus, the adsorption selectivity of a specific dye is more attractive and challenging. The above-described experiments showed that as-synthesized crystals of compounds **3** and **8** could selectively adsorb cationic dyes. As such, they would hold potential for practical application if they could still exhibit such adsorption performance in aqueous solutions that contained both dyes. Therefore, to validate whether these compounds possessed the ability to selectively adsorb MB from a blended dye solution, we tested the adsorption ability of as-synthesized crystals of compounds **3** (10 mg) and **8** (10 mg) for MB from solutions of MB/MO (40 mL, C_{MB} = 20 mg L^{-1}, C_{MO} = 20 mg L^{-1}) and MB/Apo (40 mL, C_{MB} = 20 mg L^{-1}, C_{Apo} = 30 mg L^{-1}), and examined the adsorption processes by using UV/Vis absorption spectroscopy.

When the as-synthesized crystals of compound **3** were added to mixed solutions of MB/MO and MB/Apo (Figure 12a, b), the characteristic absorption peak of MB at λ = 664 nm slowly decayed over time and almost disappeared after 60 min, whilst the absorption intensity changed from 1.51 to 0.16 for MB/MO and from 0.87 to 0.34 for MB/Apo, whereas the intensity of the absorption peak of MO or Apo only decreased slightly. Importantly, as shown in the insets in Figure 12a, b, these selective adsorptions were easily recognizable by the naked eye, as a notable change in the color of the solution from dark green to yellow for MB/MO and from reddish rose (amaranth) to pink–purple (heliotrope) for MB/Apo, following the immersion of as-synthesized crystals of compound **3** in the mixed dye solutions. The as-synthesized crystals of compound **8** exhibited similar selective-adsorption behavior for the adsorption of the mixed dye solutions under identical conditions (Figure 12c, d). Based on these findings, we concluded that the as-synthesized crystals of compounds **3** and **8** exhibited good adsorption selectivity towards MB in the dye water. Moreover, the IR spectra of compounds **3** and **8** after the selective-adsorption experiments were similar to those of the as-synthesized crystals of compounds **3** and **8**, which suggested that compounds **3** and **8** were stable during the selective adsorption of mixed dyes (see the Supporting Information, Figure S8).

3. Conclusions

In conclusion, two series of organic–inorganic hybrid DFHGMs, $[H_2INA]_2H_8[LnCu(INA)_4(H_2O)_6]_2[\alpha\text{-}GeMo_{12}O_{40}]_3\cdot 52\,H_2O$ (Ln = La^{3+} (**1**), Ce^{3+} (**2**), Pr^{3+} (**3**), Nd^{3+} (**4**), Sm^{3+} (**5**), Eu^{3+} (**6**); HINA = isonicotinic acid) and $(NH_4)[Cu(PA)_2][Cu(PA)_2Ln(H_2O)_8][\alpha\text{-}GeMo_{12}O_{40}]\cdot 10\,H_2O$ [Ln = Nd^{3+} (**7**), Sm^{3+} (**8**), Eu^{3+} (**9**); HPA = picolinic acid), have been synthesized by using a strategy that combined in situ assembly and stepwise synthesis. To the best of

our knowledge, compounds **1**–**9** represent the first plenary Keggin GMs that were functionalized by Cu–Ln–organic subunits. The dye-capture behaviors of compounds **3** and **8** (as representative examples) were systematically explored. We found that compounds **3** and **8** could efficiently and selectively adsorb MB from MO/MB or Apo/MB mixtures. Herein, we have not only demonstrated the utility of combining in situ assembly and stepwise synthesis as a synthetic method for the preparation of DFHGMs, but also significantly expanded the functional applications of DFHGMs into the realm of dye adsorption and their selective separation. Subsequent work will focus on the preparation of more neoteric DFHPOMs and exploiting their potential applications.

Experimental Section

Synthesis of $[H_2INA]_2H_8[LaCu(INA)_4(H_2O)_6]_2[\alpha\text{-}GeMo_{12}O_{40}]_3\cdot 52H_2O$ (1)

$(NH_4)_6(Mo_7O_{24})\cdot 4H_2O$ (1.002 g, 0.811 mmol) and GeO_2 (0.125 g, 1.195 mmol) were dissolved in distilled water (15 mL), the mixture was stirred for 15 min, and the pH value of the solution was adjusted to pH ≈ 1.3 by adding HCl (6 M). The mixture was stirred for 10 min then placed in a water bath at 60 °C for 30 min. Next, $CuCl_2\cdot 2H_2O$ (0.205 g, 1.202 mmol), HINA (0.074 g, 0.601 mmol), and $La(NO_3)_3\cdot 6H_2O$ (0.225 g, 0.520 mmol) were successively added and the pH value of the resulting solution was adjusted to pH ≈ 1.3 by using a dilute solution of HCl or NaOH (0.5 M). The solution was placed in a water bath at 60 °C for a further 2 h and then filtered. The filtrate was left to evaporate at ambient temperature and green block-shaped crystals of compound **1** were obtained after 2 days.

Yield: ca. 40% (based on HINA); IR (KBr): $\tilde{\nu}$ = 3434 (m), 2923 (w), 1720 (w), 1602 (s), 1405 (w), 1247 (m), 950 (s), 882 (s), 805 (s), 759 cm^{-1} (s); elemental analysis calcd (%) for $C_{60}H_{180}Cu_2Ge_3La_2Mo_{36}N_{10}O_{204}$: C 8.60, H 2.16, N 1.67, Ge 2.60, Cu 1.51, La 3.31, Mo 41.20; found: C 8.72, H 2.31, N 1.55, Ge 2.41, Cu 1.38, La 3.45, Mo 40.97.

Synthesis of $[H_2INA]_2H_8[CeCu(INA)_4(H_2O)_6]_2[\alpha\text{-}GeMo_{12}O_{40}]_3\cdot 52H_2O$ (2)

The synthesis of compound **2** was similar to that of compound **1**, except that $Ce(NO_3)_3\cdot 6H_2O$ (0.224 g, 0.516 mmol) was used instead of $La(NO_3)_3\cdot 6H_2O$ (0.225 g, 0.520 mmol). Green block-shaped crystals of compound **2** were obtained after 2 days.

Yield: ca. 42% (based on HINA); IR (KBr): $\tilde{\nu}$ = 3427 (m), 2924 (w), 1722 (m), 1598 (s), 1403 (w), 1243 (m), 952 (s), 884 (s), 804 (s), 758 cm^{-1} (s); elemental analysis calcd (%) for $C_{60}H_{180}Cu_2Ge_3Ce_2Mo_{36}N_{10}O_{204}$: C 8.59, H 2.16, N 1.67, Ge 2.60, Cu 1.52, Ce 3.34, Mo 41.19; found: C 8.73, H 2.28, N 1.53, Ge 2.44, Cu 1.40, Ce 3.48, Mo 40.99.

Synthesis of $[H_2INA]_2H_8[PrCu(INA)_4(H_2O)_6]_2[\alpha\text{-}GeMo_{12}O_{40}]_3\cdot 52H_2O$ (3)

The synthesis of compound **3** was similar to that of compound **1**, except that $Pr(NO_3)_3\cdot 6H_2O$ (0.224 g, 0.515 mmol) was used instead of $La(NO_3)_3\cdot 6H_2O$ (0.225 g, 0.520 mmol). Green block-shaped crystals of compound **3** were obtained after 2 days.

Yield: ca. 39% (based on HINA); IR (KBr): $\tilde{\nu}$ = 3428 (m), 2924 (w), 1721 (m), 1598 (s), 1404 (w), 1243 (m), 952 (s), 882 (s), 803 (s), 760 cm^{-1} (s); elemental analysis calcd (%) for $C_{60}H_{180}Cu_2Ge_3Pr_2Mo_{36}N_{10}O_{204}$: C 8.59, H 2.16, N 1.67, Ge 2.60, Cu 1.52, Pr 3.36, Mo 41.18; found: C 8.72, H 2.29, N 1.51, Ge 2.40, Cu 1.39, Pr 3.48, Mo 40.81.

Synthesis of $[H_2INA]_2H_8[NdCu(INA)_4(H_2O)_6]_2[\alpha\text{-}GeMo_{12}O_{40}]_3\cdot 52H_2O$ (4)

The synthesis of compound **4** was similar to that of compound **1**, except that $Nd(NO_3)_3\cdot 6H_2O$ (0.224 g, 0.511 mmol) was used instead of $La(NO_3)_3\cdot 6H_2O$ (0.225 g, 0.520 mmol). Green block-shaped crystals of compound **4** were obtained after 2 days.

Yield: ca. 40% (based on HINA); IR (KBr): $\tilde{\nu}$ = 3427 (m), 2925 (w), 1720 (w), 1600 (s), 1406 (w), 1246 (m), 950 (s), 883 (s), 804 (s), 756 cm^{-1} (s); elemental analysis calcd (%) for $C_{60}H_{180}Cu_2Ge_3Nd_2Mo_{36}N_{10}O_{204}$: C 8.59, H 2.16, N 1.67, Ge 2.60, Cu 1.51, Nd 3.44, Mo 41.15; found: C 8.74, H 2.29, N 1.50, Ge 2.47, Cu 1.36, Nd 3.61, Mo 40.87.

Synthesis of $[H_2INA]_2H_8[SmCu(INA)_4(H_2O)_6]_2[\alpha\text{-}GeMo_{12}O_{40}]_3\cdot 52H_2O$ (5)

The synthesis of compound **5** was similar to that of compound **1**, except that $Sm(NO_3)_3\cdot 6H_2O$ (0.224 g, 0.504 mmol) was used instead of $La(NO_3)_3\cdot 6H_2O$ (0.225 g, 0.520 mmol). Green block-shaped crystals of compound **5** were obtained after 2 days.

Yield: ca. 38% (based on HINA); IR (KBr): $\tilde{\nu}$ = 3432 (m), 2920 (w), 1721 (w), 1606 (s), 1408 (w), 1248 (m), 951 (s), 882 (s), 806 (s), 761 cm^{-1} (s); elemental analysis calcd (%) for $C_{60}H_{180}Cu_2Ge_3Sm_2Mo_{36}N_{10}O_{204}$: C 8.57, H 2.16, N 1.67, Ge 2.59, Cu 1.51, Sm 3.58, Mo 41.09; found: C 8.70, H 2.30, N 1.52, Ge 2.45, Cu 1.34, Sm 3.70, Mo 40.82.

Synthesis of $[H_2INA]_2H_8[EuCu(INA)_4(H_2O)_6]_2[\alpha\text{-}GeMo_{12}O_{40}]_3\cdot 52H_2O$ (6)

The synthesis of compound **6** was similar to that of compound **1**, except that $Eu(NO_3)_3\cdot 6H_2O$ (0.224 g, 0.502 mmol) was used instead of $La(NO_3)_3\cdot 6H_2O$ (0.225 g, 0.520 mmol). Green block-shaped crystals of compound **6** were obtained after 2 days.

Yield: ca. 36% (based on HINA); IR (KBr): $\tilde{\nu}$ = 3430 (m), 2919 (w), 1721 (w), 1606 (s), 1409 (w), 1248 (m), 951 (s), 884 (s), 807 (s), 760 cm^{-1} (s); elemental analysis calcd (%) for $C_{60}H_{180}Cu_2Ge_3Eu_2Mo_{36}N_{10}O_{204}$: C 8.57, H 2.16, N 1.67, Ge 2.59, Cu 1.51, Eu 3.61, Mo 41.07; found: C 8.69, H 2.28, N 1.51, Ge 2.46, Cu 1.35, Eu 3.76, Mo 40.88.

Synthesis of $(NH_4)[Nd(H_2O)_8][Cu(PA)_2]_2[\alpha\text{-}GeMo_{12}O_{40}]\cdot 10H_2O$ (7)

$(NH_4)_6(Mo_7O_{24})\cdot 4H_2O$ (1.005 g, 0.813 mmol) and GeO_2 (0.124 g, 1.185 mmol) were dissolved in distilled water (15 mL), the mixture was stirred for 15 min, and the pH value of the solution was adjusted to pH ≈ 1.0 by adding HCl (6 M). The mixture was stirred for 10 min and then placed in a water bath at 60 °C for 30 min. Next, $CuCl_2\cdot 2H_2O$ (0.205 g, 1.202 mmol), HPA (0.075 g, 0.609 mmol), and $Nd(NO_3)_3\cdot 6H_2O$ (0.225 g, 0.513 mmol) were successively added and the pH value of the resulting solution was adjusted to pH ≈ 1.0 by using a dilute solution of NaOH (0.5 M). The solution was placed in a water bath at 60 °C for a further 2 h and then filtered. The filtrate was left to evaporate at ambient temperature and dark-green block-shaped crystals of compound **7** were obtained after 2 days.

Yield: ca. 41% (based on HPA); IR (KBr): $\tilde{\nu}$ = 3430 (m), 1626 (s), 1600 (s), 1382 (s), 950 (s), 875 (s), 807 (s), 757 cm^{-1} (m); elemental analysis calcd (%) for $C_{24}H_{60}Cu_2GeNdMo_{12}N_5O_{68}$: C 9.60, H 2.01, N 2.33, Ge 2.42, Cu 4.23, Nd 4.80, Mo 38.35; found: C 9.76, H 2.18, N 2.21, Ge 2.29, Cu 4.10, Nd 4.95, Mo 38.12.

Synthesis of $(NH_4)[Sm(H_2O)_8][Cu(PA)_2]_2[\alpha\text{-}GeMo_{12}O_{40}]\cdot 10H_2O$ (8)

The synthesis of compound **8** was similar to that of compound **7**, except that $Sm(NO_3)_3\cdot 6H_2O$ (0.224 g, 0.504 mmol) was used instead of $Nd(NO_3)_3\cdot 6H_2O$ (0.225 g, 0.513 mmol). Dark-green block-shaped crystals of compound **8** were obtained after 2 days.

Yield: ca. 40% (based on HPA); IR (KBr): $\tilde{\nu}$ = 3433 (m), 1625 (s), 1599 (s), 1383 (s), 950 (s), 874 (s), 807 (s), 757 cm^{-1} (m); elemental analysis calcd (%) for $C_{24}H_{60}Cu_2GeSmMo_{12}N_5O_{68}$: C 9.57, H 1.99, N 2.33, Ge 2.41, Cu 4.23, Sm 5.00, Mo 38.27; found: C 9.69, H 2.17, N 2.19, Ge 2.33, Cu 4.14, Sm 5.18, Mo 37.98.

Synthesis of $(NH_4)[Eu(H_2O)_8][Cu(PA)_2]_2[\alpha\text{-}GeMo_{12}O_{40}]\cdot 10H_2O$ (9)

The synthesis of compound **9** was similar to that of compound **7**, except that $Eu(NO_3)_3\cdot 6H_2O$ (0.224 g, 0.502 mmol) was used instead of $Nd(NO_3)_3\cdot 6H_2O$ (0.225 g, 0.513 mmol). Dark-green block-shaped crystals of compound **9** were obtained after 2 days.

Yield: ca. 39% (based on HPA); IR (KBr): $\tilde{\nu}$ = 3431 (m), 1625 (s), 1599 (s), 1384 (s), 951 (s), 875 (s), 807 (s), 757 cm^{-1} (m); elemental analysis calcd (%) for $C_{24}H_{60}Cu_2GeEuMo_{12}N_5O_{68}$: C 9.57, H 1.99, N 2.33, Ge 2.41, Cu 4.22, Eu 5.05, Mo 38.25; found: C 9.70, H 2.15, N 2.16, Ge 2.27, Cu 4.11, La 5.21, Mo 37.94.

Acknowledgements

This work was supported by the Natural Science Foundation of China (21571048, 21671054, and 21771052), the Program for Science & Technology Innovation Talents in Universities of Henan Province (16HASTIT001), the Foundation of State Key Laboratory of Structural Chemistry (20160016), the 2014 Special Foundation for Scientific Research Project of Henan University (XXJC20140001), and the Students Innovative Pilot Plan of Henan University (16NA005).

Conflict of interest

The authors declare no conflict of interest.

Keywords: adsorption · dyes · germanium · heterometallic complexes · polyoxometalates

[1] a) T. Zhang, W.-B. Lin, *Chem. Soc. Rev.* **2014**, *43*, 5982–5993; b) S. Omwoma, C. T. Gore, Y.-C. Ji, C.-W. Hu, Y.-F. Song, *Coord. Chem. Rev.* **2015**, *286*, 17–29; c) J.-Z. Liao, H.-L. Zhang, S.-S. Wang, J.-P. Yong, X.-Y. Wu, R.-M. Yu, C.-Z. Lu, *Inorg. Chem.* **2015**, *54*, 4345–4350; d) P.-T. Ma, F. Hu, R. Wan, Y. Huo, D.-T. Zhang, J.-Y. Niu, J.-P. Wang, *J. Mater. Chem. C* **2016**, *4*, 5424–5433.

[2] a) H. N. Miras, G. J. T. Cooper, D.-L. Long, H. Bögge, A. Müller, C. Streb, L. Cronin, *Science* **2010**, *327*, 72–74; b) X.-L. He, Y.-P. Liu, K.-N. Gong, Z.-G. Han, X.-L. Zhai, *Inorg. Chem.* **2015**, *54*, 1215–1217.

[3] a) T. Yamase, *Chem. Rev.* **1998**, *98*, 307–326; b) M. T. Pope, A. Müller, *Angew. Chem. Int. Ed. Engl.* **1991**, *30*, 34–48; *Angew. Chem.* **1991**, *103*, 56–70; c) S.-T. Zheng, J. Zhang, J. M. Clemente-Juan, D.-Q. Yuan, G.-Y. Yang, *Angew. Chem. Int. Ed.* **2009**, *48*, 7176–7179; *Angew. Chem.* **2009**, *121*, 7312–7315.

[4] a) R. E. P. Winpenny, *Chem. Soc. Rev.* **1998**, *27*, 447–452; b) X.-P. Yang, R. A. Jones, S.-M. Huang, *Coord. Chem. Rev.* **2014**, *273–274*, 63–75; c) K. Liu, W. Shi, P. Cheng, *Coord. Chem. Rev.* **2015**, *289–290*, 74–122.

[5] a) J.-C. Liu, Q. Han, L.-J. Chen, J.-W. Zhao, *CrystEngComm* **2016**, *18*, 842–862; b) S. Reinoso, *Dalton Trans.* **2011**, *40*, 6610–6615; c) J.-W. Zhao, Y.-Z. Li, L.-J. Chen, G.-Y. Yang, *Chem. Commun.* **2016**, *52*, 4418–4445.

[6] a) C.-D. Wu, C.-Z. Lu, H.-H. Zhuang, J.-S. Huang, *J. Am. Chem. Soc.* **2002**, *124*, 3836–3837; b) H.-Y. Zhao, J.-W. Zhao, B.-F. Yang, H. He, G.-Y. Yang, *CrystEngComm* **2014**, *16*, 2230–2238; c) S.-S. Shang, J.-W. Zhao, L.-J. Chen, Y.-Y. Li, J.-L. Zhang, Y.-Z. Li, J.-Y. Niu, *J. Solid State Chem.* **2012**, *196*, 29–39.

[7] H. Xue, Z. Zhang, R. Pan, B.-F. Yang, H.-S. Liu, G.-Y. Yang, *CrystEngComm* **2016**, *18*, 4643–4650.

[8] G.-L. Xue, B. Liu, H.-M. Hu, J.-H. Yang, J.-W. Wang, F. Fu, *J. Mol. Struct.* **2004**, *690*, 95–103.

[9] a) A. Merca, A. Müller, J. V. Slageren, M. Läge, B. Krebs, *J. Cluster Sci.* **2007**, *18*, 711–719; b) X.-K. Fang, P. Kögerler, *Angew. Chem. Int. Ed.* **2008**, *47*, 8123–8126; *Angew. Chem.* **2008**, *120*, 8243–8246; c) X.-K. Fang, P. Kögerler, *Chem. Commun.* **2008**, 3396–3398; d) J.-P. Wang, Q.-X. Yan, X.-D. Du, J.-Y. Niu, *Chin. J. Chem.* **2008**, *26*, 1239–1243; e) B. Li, J.-W. Zhao, S.-T. Zheng, G.-Y. Yang, *J. Cluster Sci.* **2009**, *20*, 503–513; f) D.-Y. Du, J.-S. Qin, S.-L. Li, X.-L. Wang, G.-S. Yang, Y.-G. Li, K.-Z. Shao, Z.-M. Su, *Inorg. Chim. Acta* **2010**, *363*, 3823–3831; g) D.-Y. Du, J.-S. Qin, G. Yuan, Y.-Q. Lan, X.-L. Wang, K.-Z. Shao, Z.-M. Su, *Solid State Sci.* **2011**, *13*, 1115–1121; h) L.-J. Chen, D.-Y. Shi, Y. Wang, H.-L. Cheng, Z.-D. Geng, J.-W. Zhao, P.-T. Ma, J.-Y. Niu, *J. Coord. Chem.* **2011**, *64*, 400–412; i) D.-Y. Shi, L.-J. Chen, J.-W. Zhao, Y. Wang, P.-T. Ma, J.-Y. Niu, *Inorg. Chem. Commun.* **2011**, *14*, 324–329; j) J. Luo, C.-L. Leng, L.-J. Chen, J. Yuan, H.-Y. Li, J.-W. Zhao, *Synth. Met.* **2012**, *162*, 1558–1565; k) D.-Y. Shi, J.-W. Zhao, L.-J. Chen, P.-T. Ma, J.-P. Wang, J.-Y. Niu, *CrystEngComm* **2012**, *14*, 3108–3119; l) J.-W. Zhao, D.-Y. Shi, L.-J. Chen, Y.-Z. Li, P.-T. Ma, J.-P. Wang, J.-Y. Niu, *Dalton Trans.* **2012**, *41*, 10740–10751; m) S.-W. Zhang, J.-W. Zhao, P.-T. Ma, H.-N. Chen, J.-Y. Niu, J.-P. Wang, *Cryst. Growth Des.* **2012**, *12*, 1263–1272; n) J.-W. Zhao, D.-Y. Shi, L.-J. Chen, P.-T. Ma, J.-P. Wang, J. Zhang, J.-Y. Niu, *Cryst. Growth Des.* **2013**, *13*, 4368–4377; o) J.-W. Zhao, Y.-Z. Li, F. Ji, J. Yuan, L.-J. Chen, G.-Y. Yang, *Dalton Trans.* **2014**, *43*, 5694–5706; p) L.-J. Chen, J. Cao, X.-H. Li, X. Ma, J. Luo, J.-W. Zhao, *CrystEngComm* **2015**, *17*, 5002–5013; q) J.-W. Zhao, J. Cao, Y.-Z. Li, J. Zhang, L.-J. Chen, *Cryst. Growth Des.* **2014**, *14*, 6217–6229; r) L.-J. Chen, F. Zhang, X. Ma, J. Luo, J.-W. Zhao, *Dalton Trans.* **2015**, *44*, 12598–12612; s) J. Luo, G. F. Jin, F. Zhang, Y. Liu, L. J. Chen, S. Q. Xie, J. W. Zhao, *Eur. J. Inorg. Chem.* **2018**, 143–152; t) J. Cai, X.-Y. Zheng, J. Xie, Z.-H. Yan, X.-J. Kong, Y.-P. Ren, L.-S. Long, L.-S. Zheng, *Inorg. Chem.* **2017**, *56*, 8439–8445; u) Y.-N. Gu, Y. Chen, Y.-L. Wu, S.-T. Zheng, X.-X. Li, *Inorg. Chem.* **2018**, *57*, 2472–2479.

[10] J.-W. Zhao, J.-L. Zhang, Y.-Z. Li, J. Cao, L.-J. Chen, *Cryst. Growth Des.* **2014**, *14*, 1467–1475.

[11] a) X.-J. Feng, W.-Z. Zhou, Y.-G. Li, H.-S. Ke, J.-K. Tang, R. Clérac, Y.-H. Wang, Z.-M. Su, E.-B. Wang, *Inorg. Chem.* **2012**, *51*, 2722–2724; b) J. D. Compain, K. Nakabayashi, S. Ohkoshi, *Inorg. Chem.* **2012**, *51*, 4897–4899.

[12] S.-W. Zhang, K. Wang, D.-D. Zhang, P.-T. Ma, J.-Y. Niu, J.-P. Wang, *CrystEngComm* **2012**, *14*, 8677–8683.

[13] a) R. C. Howell, F. G. Perez, S. Jain, W. D. Horrocks, A. L. Rheingold, L. C. Francesconi, *Angew. Chem. Int. Ed.* **2001**, *40*, 4031–4034; *Angew. Chem.* **2001**, *113*, 4155–4158; b) X.-L. Wang, Y.-Q. Guo, Y.-G. Li, E.-B. Wang, C.-W. Hu, N.-H. Hu, *Inorg. Chem.* **2003**, *42*, 4135–4140.

[14] a) A. J. Gaunt, I. May, D. Collison, O. D. Fox, *Inorg. Chem.* **2003**, *42*, 5049–5051; b) J.-W. Zhao, H.-L. Li, Y.-Z. Li, C.-Y. Li, Z.-L. Wang, L.-J. Chen, *Cryst. Growth Des.* **2014**, *14*, 5495–5505.

[15] B. Li, J.-W. Zhao, S.-T. Zheng, G.-Y. Yang, *Inorg. Chem.* **2009**, *48*, 8294–8303.

[16] R. G. Pearson, *J. Am. Chem. Soc.* **1963**, *85*, 3533–3539.

[17] P.-J. Gong, Y.-Y. Li, C.-P. Zhai, J. Luo, X.-M. Tian, L.-J. Chen, J.-W. Zhao, *CrystEngComm* **2017**, *19*, 834–852.

[18] Y.-F. Zhou, M.-C. Hong, X.-T. Wu, *Chem. Commun.* **2006**, 135–143.

[19] a) I. D. Brown, D. Altermatt, *Acta Crystallogr. Sect. B* **1985**, *41*, 244–247; b) H. H. Thorp, *Inorg. Chem.* **1992**, *31*, 1585–1588; c) A. Trzesowska, R. Kruszynski, T. J. Bartczak, *Acta Crystallogr. Sect. B* **2004**, *60*, 174–178.

[20] a) P.-J. Gong, G.-F. Jin, C.-T. Lu, L.-J. Chen, J.-W. Zhao, *Inorg. Chem. Commun.* **2017**, *83*, 1 – 6; b) X.-L. Wang, N. Li, A.-X. Tian, J. Ying, G.-C. Liu, H.-Y. Lin, J.-W. Zhang, Y. Yang, *Dalton Trans.* **2013**, *42*, 14856 – 14865.
[21] a) H.-Y. Zhao, J.-W. Zhao, B.-F. Yang, H. He, G.-Y. Yang, *CrystEngComm* **2013**, *15*, 8186 – 8194; b) J.-W. Zhao, J. Luo, L.-J. Chen, J. Yuan, H.-Y. Li, P.-T. Ma, J.-P. Wang, J.-Y. Niu, *CrystEngComm* **2012**, *14*, 7981 – 7993; c) J.-F. Cao, S.-X. Liu, R.-G. Cao, L.-H. Xie, Y.-H. Ren, C.-Y. Gao, L. Xu, *Dalton Trans.* **2008**, 115 – 120.
[22] a) G. Crini, *Bioresour. Technol.* **2006**, *97*, 1061 – 1085; b) A. Bafana, S. S. Devi, T. Chakrabarti, *Environ. Rev.* **2011**, *19*, 350 – 371.
[23] H. Zhang, D. Chen, X.-J. Lv, Y. Wang, H.-X. Chang, J.-H. Li, *Environ. Sci. Technol.* **2010**, *44*, 1107 – 1111.
[24] a) H.-X. Yang, T.-F. Liu, M.-N. Cao, H.-F. Li, S.-Y. Gao, R. Cao, *Chem. Commun.* **2010**, *46*, 2429 – 2431; b) L. Young, J. Yu, *Water Res.* **1997**, *31*, 1187 – 1193.
[25] Q.-R. Fang, G.-S. Zhu, Z. Jin, Y.-Y. Ji, J.-W. Ye, M. Xue, H. Yang, Y. Wang, S.-L. Qiu, *Angew. Chem. Int. Ed.* **2007**, *46*, 6638 – 6642; *Angew. Chem.* **2007**, *119*, 6758 – 6762.
[26] a) J. Lü, X.-J. Lin, X.-L. Zhao, R. Cao, *Chem. Commun.* **2012**, *48*, 669 – 671; b) Y. Hu, F. Luo, F.-F. Dong, *Chem. Commun.* **2011**, *47*, 761 – 763.
[27] a) X.-L. Wang, Q. Gao, A.-X. Tian, G.-C. Liu, *Cryst. Growth Des.* **2012**, *12*, 2346 – 2354; b) A.-X. Yan, S. Yao, Y.-G. Li, Z.-M. Zhang, Y. Lu, W.-L. Chen, E.-B. Wang, *Chem. Eur. J.* **2014**, *20*, 6927 – 6933; c) F.-Y. Yi, W. Zhu, S. Dang, J.-P. Li, D. Wu, Y.-H. Wu, Z.-M. Sun, *Chem. Commun.* **2015**, *51*, 3336 – 3339.
[28] a) A. Çelekli, H. Bozkurt, *Environ. Sci. Pollut. Res.* **2013**, *20*, 4647 – 4658; b) X.-L. Wang, X. Rong, H.-Y. Lin, D.-N. Liu, X. Wang, G.-C. Wang, G. Song, *Inorg. Chim. Acta* **2017**, *461*, 279 – 289.
[29] L. Liu, B. Wang, J.-H. Lv, K. Yu, L. Wang, H. Zhang, S. Wang, B.-B. Zhou, *CrystEngComm* **2017**, *19*, 5653 – 5661.
[30] L. Li, X.-L. Liu, H.-Y. Geng, B. Hu, G.-W. Song. Z.-S. Xu, *J. Mater. Chem. A.* **2013**, 1, 10292 – 10299.
[31] L.-L. Lv, J. Yang, H.-M. Zhang, Y.-Y. Liu, J.-F. Ma, *Inorg. Chem.* **2015**, *54*, 1744 – 1755.
[32] a) S. Dawood, T. K. Sen, *Water Res.* **2012**, *46*, 1933 – 1946; b) D. K. Mahmoud, M. A. M. Salleh, W. A. W. A. Karim, A. Idris, Z. Z. Abidin, *Chem. Eng. J.* **2012**, *181 – 182*, 449 – 457; c) J.-W. Fu, Z.-H. Chen, X.-C. Wu, M.-H. Wang, X.-Z. Wang, J.-H. Zhang, J.-A. Zhang, Q. Xu, *Chem. Eng. J.* **2015**, *281*, 42 – 52.
[33] a) X.-L. Wang, G. Song, H.-Y. Lin, X. Wang, G.-C. Liu, X. Rong, *CrystEngComm* **2018**, *20*, 51 – 62; b) J.-S. Yan, K.-N. Gong, X.-L. Xue, X.-L. He, C. Zhao, Z.-G. Han, H.-T. Yu, *Eur. J. Inorg. Chem.* **2014**, 5969 – 5976; c) X.-X. Liu, W.-P. Gong, J. Luo, C.-T. Zou, Y. Yang, S.-J. Yang, *Appl. Surf. Sci.* **2016**, *362*, 517 – 524; d) C. Zou, Z.-J. Zhang, X. Xu, Q.-H. Gong, J. Li, C.-D. Wu, *J. Am. Chem. Soc.* **2012**, *134*, 87 – 90; e) Y.-J. Yao, F.-F. Xu, M. Chen, Z.-X. Xu, Z.-W. Zhu, *Bioresour. Technol.* **2010**, *101*, 3040 – 3046; f) C. D. Woolard, J. Strong, C. R. Erasmus, *Appl. Geochem.* **2002**, *17*, 1159 – 1164; g) E. E. Baldez, N. F. Robaina, R. J. Cassella, *J. Hazard. Mater.* **2008**, *159*, 580 – 586; h) R. Li, X.-Q. Ren, J.-S. Zhao, X. Feng, X. Jiang, X.-X. Fan, Z.-G. Lin, X.-G. Li, C.-G. Hu, B. Wang, *J. Mater. Chem. A* **2014**, *2*, 2168 – 2173.
[34] M. Ghaedi, A. Hassanzadeh, S. N. Kokhdan, *J. Chem. Eng. Data* **2011**, *56*, 2511 – 2520.
[35] a) A. Salifu, B. Petrusevski, K. Ghebremichael, L. Modestus, R. Buamah, C. Aubry, G. L. Amy, *Chem. Eng. J.* **2013**, *228*, 63 – 74; b) X.-P. Liao, B. Shi, *Environ. Sci. Technol.* **2005**, *39*, 4628 – 4632.

Manuscript received: August 18, 2018
Revised manuscript received: September 10, 2018
Accepted manuscript online: September 11, 2018
Version of record online: October 31, 2018